Mapping Volcanism and Tectonism of the Slow-Spreading Lucky Strike Segment (Mid-Atlantic Ridge, 37°17′N)

D. Samantha Nakata

Senior Integrative Exercise

11 April 2008

Submitted in partial fulfillment of the requirements for a Bachelor of Arts, Geology degree from Carleton College, Northfield, Minnesota.

TABLE OF CONTENTS

Mapping Volcanism and Tectonism of the Slow-Spreading Lucky Strike Segment (Mid-Atlantic Ridge, 37°17′N)

D. Samantha Nakata
Carleton College
Senior Integrative Exercise
11 April 2008

Advisors:
S. Adam Soule, Woods Hole Oceanographic Institution
Bereket Haileab, Carleton College

ABSTRACT

Existing high-resolution sidescan sonar and multibeam bathymetry data, coupled with ~17,000 recently collected seafloor images, are used to identify volcanic and tectonic features of the median valley floor of the slow-spreading Lucky Strike segment of the Mid-Atlantic Ridge (37°23′-37°13′N). Mapping of the area demonstrates a normal distribution of flow types. The most recent volcanic activity was emplaced along axis, south of the seamount summit cones. Based on the high proportion of sheet to pillow flows (36% to 64%), the Lucky Strike segment center exhibits volcanic properties more typical of an intermediate- to fast-spreading ridge. The active faulting zone spans 5-7 km across axis and accommodates more than 19% of across-axis extension. Faulting suggests that tectonic extension is accumulated asymmetrically, with eastern faults localized closer to the axis

Using analysis of sediment cover and location of fault scarps, I reconstruct the geologic history of volcanic and tectonic activity for the central portion of the Lucky Strike segment. Construction of the segment's central seamount ended 20-33 ka. Subsequent faulting of the seamount resulted in a 3-4 km wide axial graben, which confines two bands of flow that were emplaced 3-20 ka. The youngest flows must have been erupted within the last 3 kyr; these flows include construction of a pillow ridge southwest of the seamount and voluminous sheet flows confined to the axial graben in the southern region of the platform. The youngest feature is the lava lake, which overprints axis-parallel faults through the seamount and hosts an active hydrothermal field.

Keywords: Mid-Atlantic Ridge, mid-oceanic ridge, magmatism, extension, seamounts

INTRODUCTION

Located thousands of meters below the ocean surface, mid-ocean ridges and their magma sources are particularly difficult systems to study. While much progress has been made towards understanding fast-spreading ridges, this is arguably less true of slow-spreading counterparts. The highly tectonized seafloor associated with these slow-spreading segments has imposed an added obstacle to such research as surface mapping and magma source imaging. Over the past decades ocean scientists have had to formulate innovative methods and means to analyze the processes that comprise the global ridge system. Using fine-scale observations of seafloor surface features, this study aims to better characterize the volcanic and tectonic processes influencing slow-spreading ridges. In particular, I focus on Lucky Strike, a segment noted for its classification as a slow-spreading ridge and its proximity to the Azores hotspot (Fig. 1).

Previous Studies

Previous studies have undertaken surface mapping of Lucky Strike using sidescan sonar data, seafloor images, and submersible observations. With an active hydrothermal field situated at the segment center, Lucky Strike has been of special interest to hydrothermal vent research groups. Ondreas et al. (1997) and Humphris et al. (2002) have characterized rock type, sediment cover, hydrothermal deposits and vent sites in the hydrothermal field. An acoustic survey by Scheirer et al. (2000) has provided large-scale mapping of the Lucky Strike segment center. Analysis includes identification of large-scale acoustic texture variations and inferred geologic interpretations (i.e. sediment cover, constructional features, and faulting) for these textures.

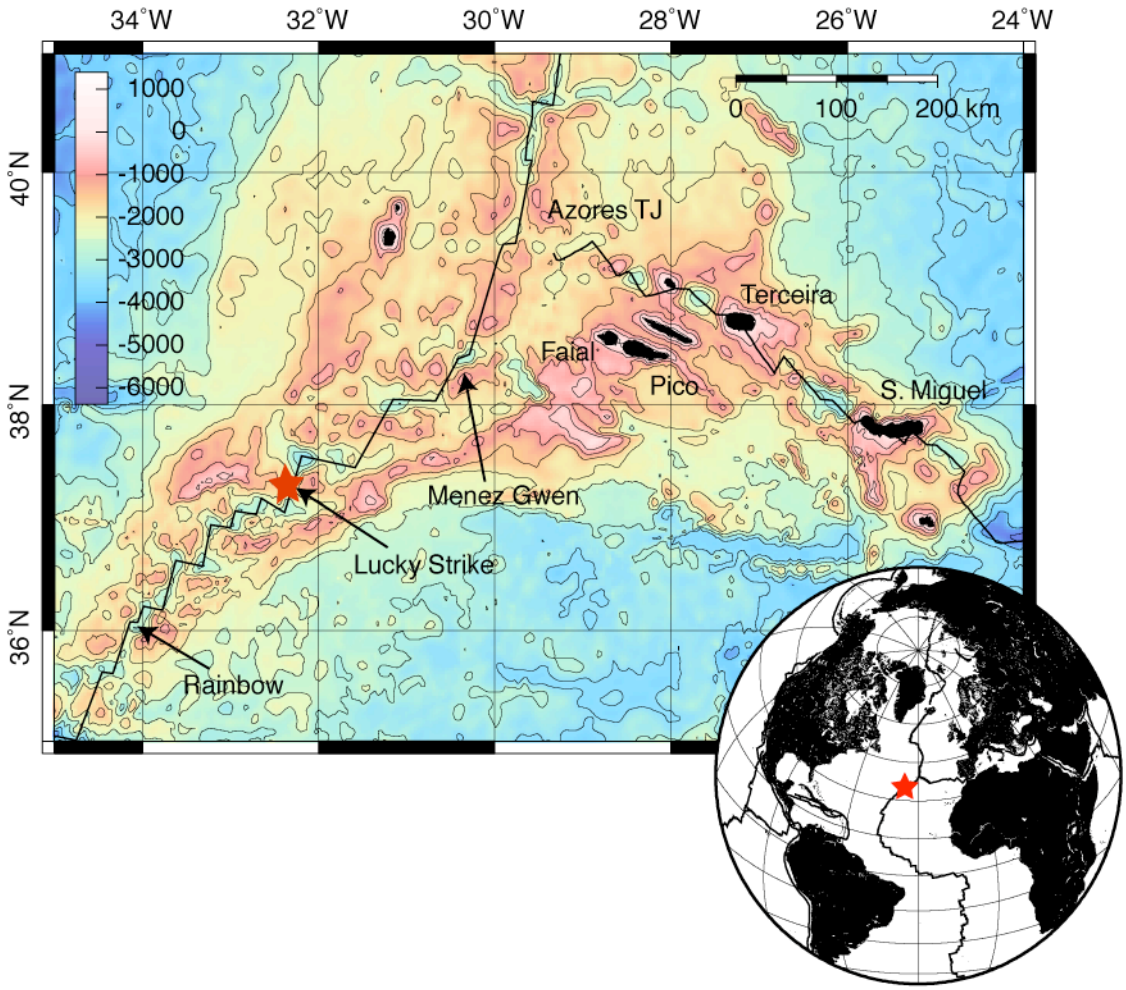

Figure 1. Lucky Strike segment indicated by the red star. Globe (bottom-right corner): location of the study area on the southwest arm of the Azores Triple Junction, along the Mid-Atlantic Ridge between 37º14'-37º23'N. Main figure: bathymetry of the area south of the Azores Triple Junction. Segments are bound at their ends by right-stepping non-transform offsets.

In 2006, a 3-D seismic reflection survey located the axial magma chamber beneath the Lucky Strike seamount (Singh et al., 2006); the axial magma chamber lies at 3 km depth (up to twice as deep as under fast spreading ridges (e.g. Kent et al., 1993)) and shallows to the south. The lens extends 7 km along axis and was has a width of 3-4 km. Lucky Strike is one of the first slow-spreading ridges at which an axial magma chamber has been successfully located.

Objectives

The goal of this study was to map the plan view distribution of volcanic and tectonic features on the axial floor of Lucky Strike and investigate patterns with respect to the known magma body at the segment center. We used DSL-120 sidescan sonar data, multibeam bathymetry, and seafloor photographs to map the sediment cover and volcanic morphologies. The resulting geologic map encompasses an area larger than that surveyed by Ondreas et al. (1997) and Humphris et al. (2002), but with observations at a finer scale than in Scheirer et al. (2000). Using these data sets and the geologic map, we investigated the along-axis and across-axis trends in volcanism, focusing specifically on how magmatic processes vary with distance from the accretionary axis and magma source. Ultimately, these observations allowed me to reconstruct a geologic history of the primary volcanic and tectonic features of the area. To a lesser extent, this study also used the sidescan sonar data and images to map faulting within the rift valley and to quantify tectonic elongation.

GEOLOGIC SETTING

Classified as a slow-spreading ridge, Lucky Strike has a full spreading rate of 22 mm/yr. The segment is 60 km long, bound at its ends by right stepping non-transform offsets (Gracia and Escartin, 1999; Parson et al., 2000). The 11-km wide axial valley encompasses one of the largest central seamounts along the MAR (Singh et al., 2006). The seamount is 6 km wide and 8 km long at its base, and shoals from 2000 m to 1600 m depth. Atop the seamount platform are four volcanic edifices: three cones on the summit of Lucky Strike, and a north-trending volcanic ridge in the NW quadrant of the platform, all of which are faulted. The three cones surround a young, unfaulted lava lake and the previously mentioned hydrothermal system (Langmuir et al., 1997; Ondreas et al., 1997; Humphris et al., 2002). My survey area is 16 km along axis and 9 km across axis, containing the rift valley floor above and around the seamount platform.

Located less than 500 km SW of the Azores Triple Junction center, Lucky Strike is proximal to the Azores hotspot. The segments near this upwelling system show a decreasing influence (both chemically and thermally) with increasing distance from the hotspot that is expressed physically, for example, by the decrease in average crustal thickness southward (Escartin et al., 2001). The decrease in thermal influence with distance from the Azores hotspot can also be traced by surface features along segment centers. Axial (topographic) highs, indicative of a continuous magma source, are observed along segments between the hotspot (~40°N) and Lucky Strike's center (37°17′N); southward, segments are characterized by axial valleys (topographic lows) (Escartin et al., 2001). The Lucky Strike Seamount, reaching 1600 m depth, is an axial high; the ridge represents the extent of influence by the Azores hotspot along the

southwest arm of the triple junction. Segments south of Lucky Strike can therefore be considered more typical representatives of the slow-spreading MAR.

The presence of a large axial seamount and an active hydrothermal field at Lucky Strike provide evidence for local magmatic robustness, although some degree of central magma focusing in not uncommon in this region of the MAR (Escartin et al., 2001; Cann and Smith, 2005). The findings of this study may prove useful in determining whether the segment's surface morphology is a result of the hotspot interaction, or merely central magma focusing.

DATA SOURCES

Bathymetry was used to identify large-scale topographic features, particularly the bounding faults of the rift valley, the base of the seamount platform, and the northwest volcanic ridge and summit cones constructed above the platform (Fig. 2a). The multibeam bathymetry data have a 40-m/pixel grid resolution (Fouquet, pers. comm.).

The sidescan sonar data (Fig. 2b) were collected in 1996 during the LUSTRE '96 cruise (Fornari and Humphris, 1996) using the Woods Hole Oceanographic Institution's DSL-120. The instrument was towed 100 m above the seafloor at ~1 knot, providing a swath width of 1 km. The nadir (25 m wide area directly beneath the tow line) and the outermost 100 m of the swaths are the areas of lowest-quality data. The 1996 survey consists of 18 main swaths (10 in the north, and 8 in the south) running approximately parallel to the strike of the axial valley bounding faults. The sidescan images have a 4-m grid resolution and navigational precision of 10-20 m (Scheirer et al., 2000).

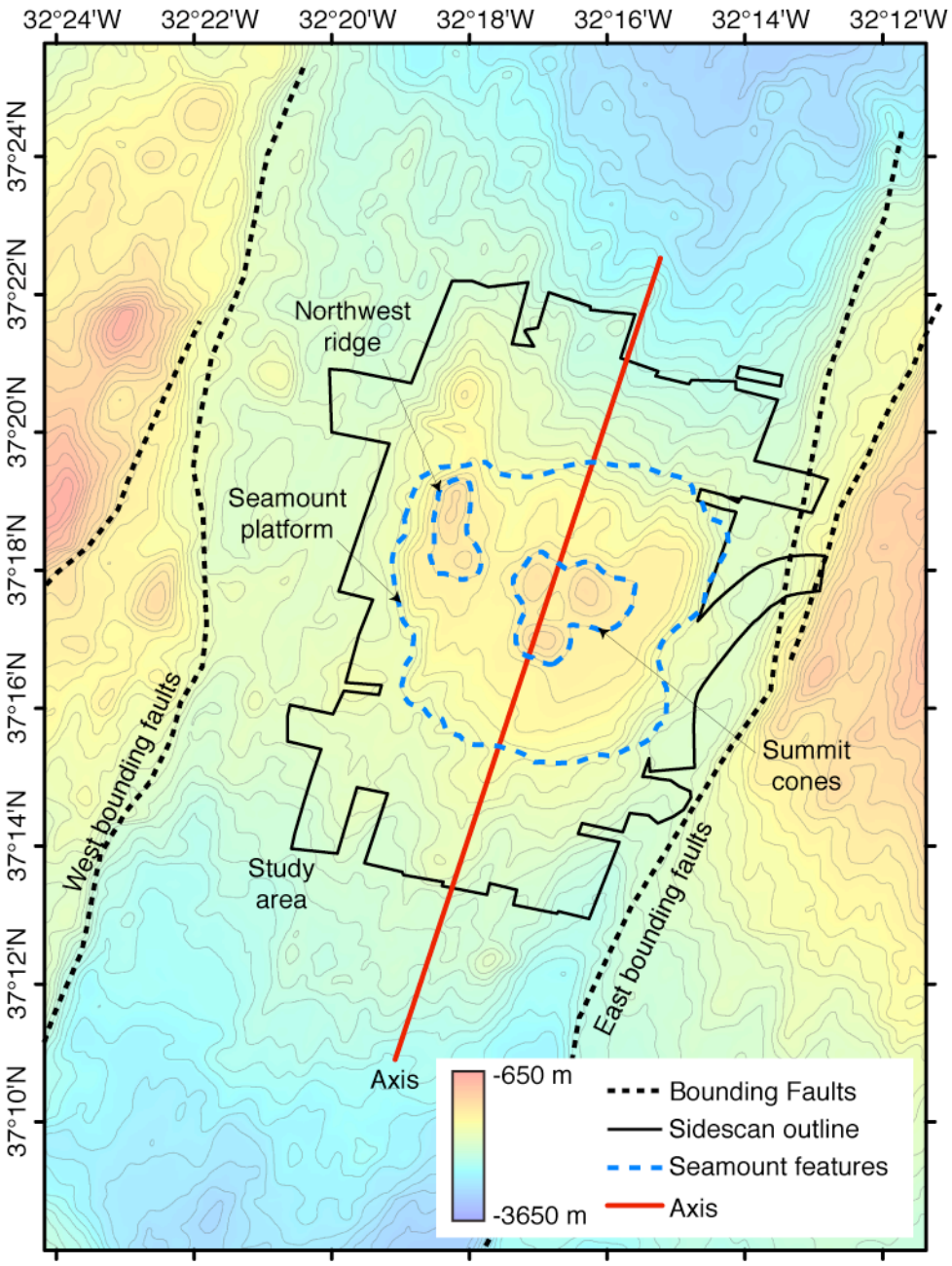

Figure 2a. Multibeam bathymetry data of and around the sidescan sonar area. Contour lines are 50 m intervals. Color change indicates depth. b. High-resolution DSL-120 sidescan sonar data: white areas are high backscatter, and darker areas are low backscatter. From north to south, the tow numbers are CT06, CT01, CT08, CT05, CT09, CT02, CT04, CT03, CT07, CT10 (shown as red lines). The white dashed box indicates the perimeter of Figure 3.

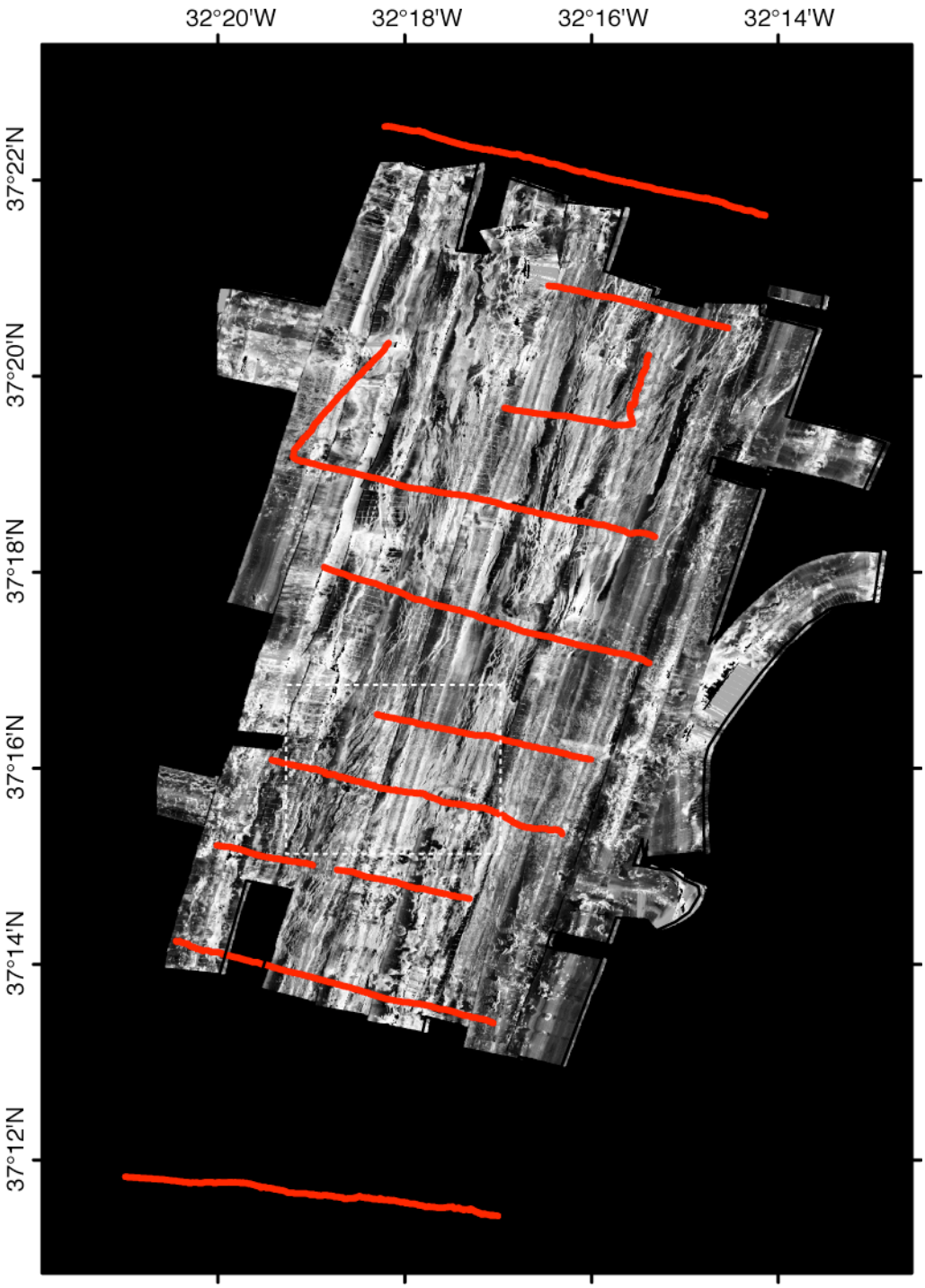
32°20'W
32°18'W
32°16'W
32°14'W
37°22'N
37°20'N
37°18'N
37°16'N
37°14'N
37°12'N

Figure 2b.

Previous mapping of the Lucky Strike segment from the same sidescan survey was reported by Scheirer et al. (2000) and Humphris et al. (2002); note that the sidescan has been reprocessed for this study.

The sidescan sonar and multibeam bathymetry data are supplemented by seafloor photographs collected in 2006 using the Woods Hole Oceanographic Institute's TowCam (Escartin et al., 2006). There are 10 across-axis tow lines (CT01 to CT10), running perpendicular to the strike of the ridge (~N020°) (Fig. 2b); two camera tows contain segments running sub-parallel to the axis: a portion of the CT05 track, ~4 km west of the axis, captures the north-trending ridge on the northwest edge of the seamount platform; part of the CT08 track, 1 km east of the axis images an area of multiple flow boundaries. Each track is 3-6 km in length, providing a total of 48 km of track line along which images were collected. Collection of these seafloor photos resulted in 16,761 usable images, taken at ~13 s intervals. The field of view for each photograph is 4-6 m; this width changes as the distance between the camera and seafloor varies. Photographs taken along scarps and high relief areas generally result in larger frame widths or blackened photos as the camera was pulled off the bottom to avoid obstacles.

During March 2001, between collection of the sidescan data and TowCam images, a hydrophone array recorded a 29-hour earthquake swarm at the Lucky Strike segment (Dziak et al., 2004). The event was interpreted as a dike intrusion, although this may not have resulted in the emplacement of lava at the seafloor. The earthquake swarm resulted in an estimated 1.7 mm of horizontal extension, which is minor compared to previously documented seismic extension events at slow-spreading ridges. We conduct

this study, using the images to ground truth the sidescan results, assuming the effects of the earthquake swarm have had little effect at the seafloor surface.

GEOGRAPHIC DISTRIBUTION OF VOLCANISM

Methods

Sidescan Sonar

The reflectivity recorded by the sidescan images relate to sediment cover, relief, and roughness of the seafloor. At slow spreading ridges, the tectonic fabric contributes to very rough topography and thus to a high range of backscatter on sidescan data. As such, acoustic facies are often difficult to interpret as much of the dynamic range results from variations in seafloor slope rather than sediment variations. However, using camera images, we are in fact able to characterize sediment cover and volcanic morphology for a given acoustic texture.

Previous mapping studies using sidescan sonar data have been able to attribute geologic interpretations to acoustic textures at a broad scale. The main acoustic textures within the Lucky Strike DSL-120 survey, which are described below, can be seen in Figure 3 in more detail.

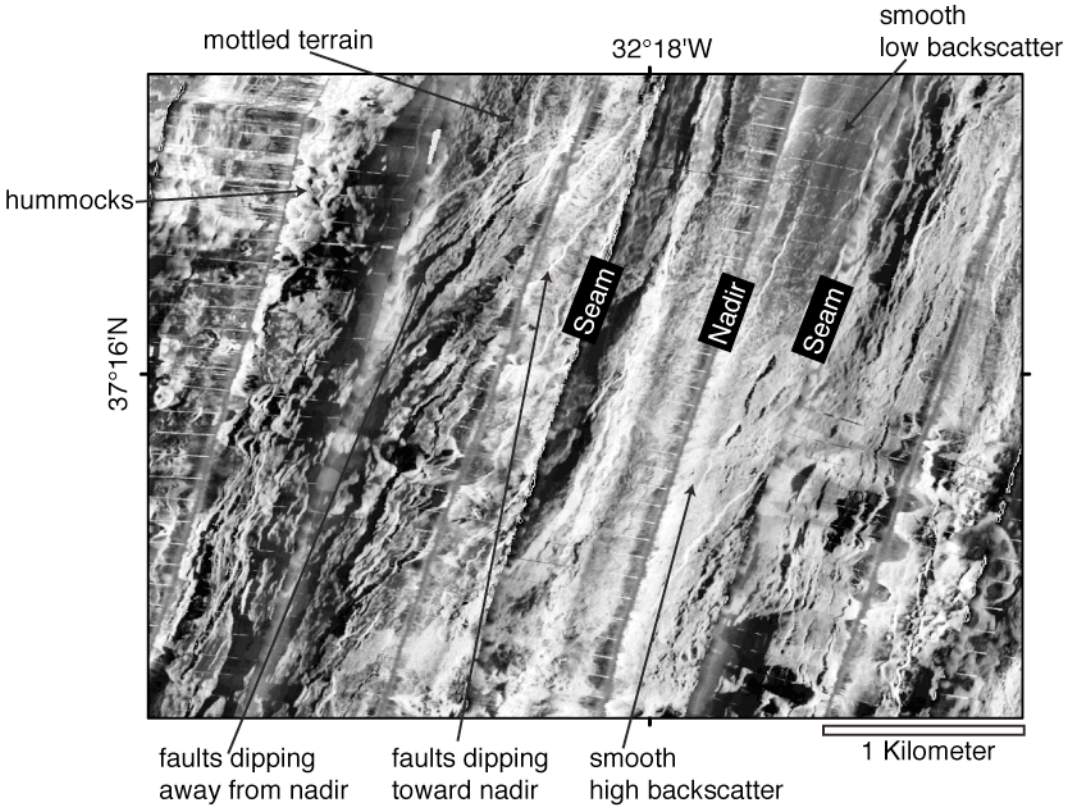

Figure 3. Inset from Figure 2a. DSL-120 sidescan sonar, with insonification from the east, showing acoustic textures found in the study area.

Hummocks are conglomerates of pillow mounds that appear acoustically as nodular regions. Individual pillow mounds are 50-200 m wide and reach heights of 200 m or more (Cann and Smith, 2005). Hummocky regions appear in sidescan sonar images as highly reflective terrains, a result of their high relief and the lack of sediment cover over these structures. Insonification of hummocks often results in shadows on the lee-side (opposite the DSL-120). In the study area, these features are the dominant acoustic texture south of the seamount platform (37°16′N). Hummocks are also observed to a lesser degree in the northwest quadrant of the survey area, beyond the perimeter of the seamount platform. Lower-backscatter hummocks are found intermittently in the southeast, as well (also beyond the perimeter of the seamount platform); the lower reflectivity may be an indication that the hummocks are relatively older, more heavily sedimented volcanic constructions.

Smooth textures may have low or high backscatter, but generally do not contain the internal structure observed in hummocks. Low-backscatter regions are often characterized by highly sedimented areas (Mitchell, 1993) where the sediment has blanketed volcanic and tectonic features, obscuring the original surface roughness. These darker, less reflective areas are found at the west and east edges of the sidescan survey. In contrast, high backscatter, uniform textures typically relate to some form of volcanic emplacement. Cann and Smith (2005) noted that smooth textures could be the acoustic expression of low-lying flows of no particular volcanic morphology; that is, sheet flows could have the same sidescan expression as pillows, which are less typically emplaced as low-lying flows. Smooth, highly reflective textures are primarily found in the northwest

quadrant of the sidescan, on the east and west flanks of the seamount platform, and at the axis.

Mottled terrain refers to patchy, intermediate backscatter. Parson et al. (2000) observed this texture at the flanks of large volcanic edifices in non-transform offsets along the MAR. In this region, mottled terrain is observed in the eastern-most 2 km of the study area, particularly the southern region, and interpreted as new lobate or sheet flows (Scheirer et al., 2000) based on the results of dredging.

Fault scarps appear as very bright or dark linear features due to reflection from talus (Searle et al., 1998) and their high relief. Scarps that dip away from the DSL-120 track line appear as sharply defined shadows because of the lack of sonar reflection. Flow boundaries are defined by both the acoustic textures and image analyses. Ideally, the area within a flow boundary correlates to a uniform texture and the dominant classification of sediment cover and morphology for the images overlying that area. Each boundary generally represents one flow episode, although acoustic facies that represent a single, older eruptive unit are sometimes disrupted by faults and younger flows.

TowCam Image Analysis

Whereas other Lucky Strike surveys have made spatially limited visual observations or have only had sidescan sonar data to make geologic interpretations from, our comprehensive camera tow data allow us to ground-truth geologic interpretations of the small-scale sidescan textures over a large area. Furthermore, the completeness of the camera tow data set act as a means of calibrating the sidescan textures and backscatter range. Variations in backscatter intensity are caused by overall seafloor roughness as well as variations in rock type and sediment cover; using seafloor photos, I could infer

the volcanic morphology and sediment cover for a particular texture that might otherwise be ambiguous.

Each photograph was classified based on sediment cover. Sediment cover in the area varies from completely unsedimented areas to completely sedimented areas (Fig. 4). The images were categorized into four levels of sedimentation. 'Completely unsedimented' areas ranged from the appearance of completely bare rock to slightly 'dusted' rocks or flows with sediment in crevices (~0% sediment). Frames that were dominantly composed of rock (<50% sediment), with some overlying sediment were classified as 'low sediment areas. 'High sediment' regions were those comprised mostly of sediment with some intruding rock surfaces (>50% sediment). 'Completely sedimented' areas show no outcropping of rock (~100% sediment). Sediment classification is significant in that it allows relative age relationships to be made between regions. Older units, which have had more time to collect sediment, will have a higher percentage of sediment cover.

Along with sedimentation level, each photograph was also classified by volcanic morphology type. Submarine lava flow surface morphologies are primary indicators of eruption style and dynamics (Gregg and Fink, 1995; Perfit and Chadwick, 1998). Mid-ocean ridge eruptions are generally classified by three morphology types: pillows, lobates and sheet flows (Fig. 5). Pillows are the dominant morphology found at slow-spreading ridges of the MAR. These flows signify low effusion rates relative to lobate and sheet flows, and are closely linked to areas with low-magma budgets where the eruptions are slow and intermittent. Sheet flows, in contrast, are emplaced with either a rough, jumbled texture or as a smoother, ropy texture.

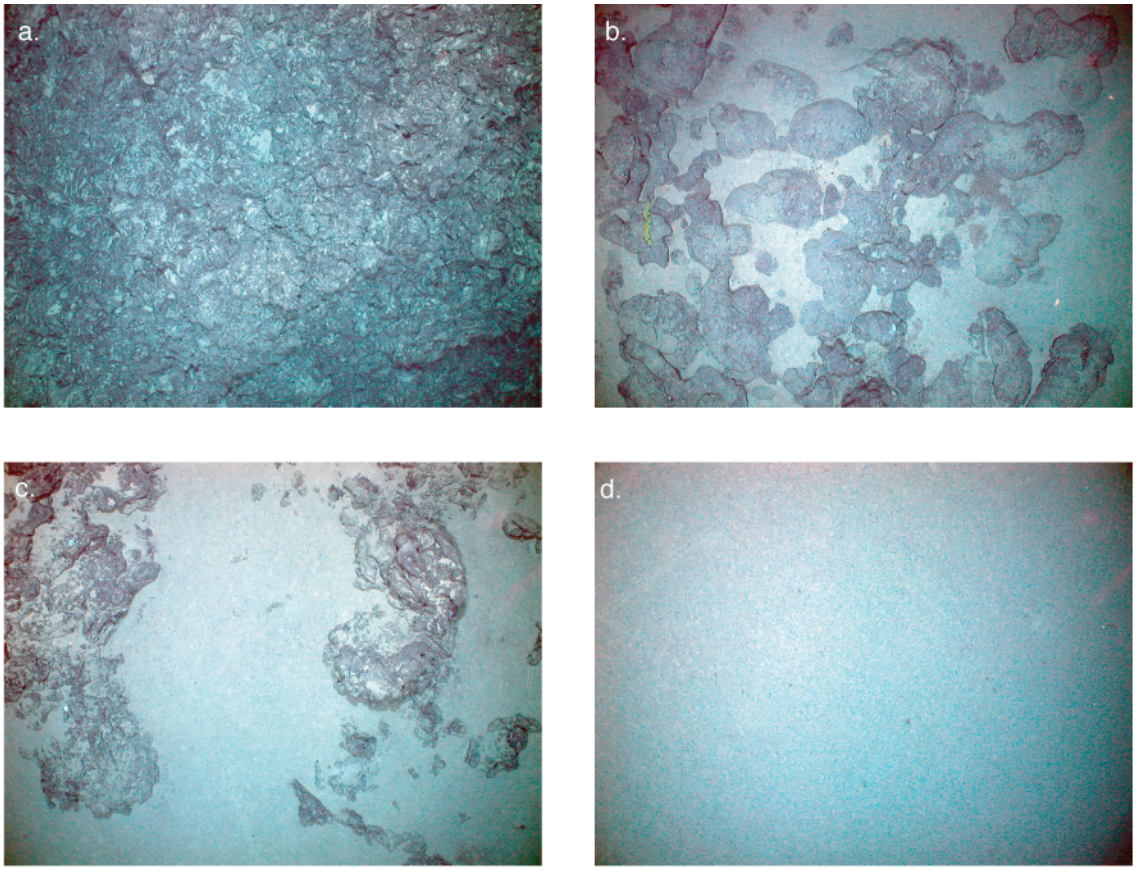

Figure 4. Four camera-tow images showing the levels of sediment classification. a. 'Completely undsedimented,' although sediment sometimes fills rock crevices. b. 'Low sediment,' with >50% outcropping of rock. c. 'High sediment' characterized by <50% rock surfaces. d. 'Completely sedimented' with no distinguishable rock surfaces.

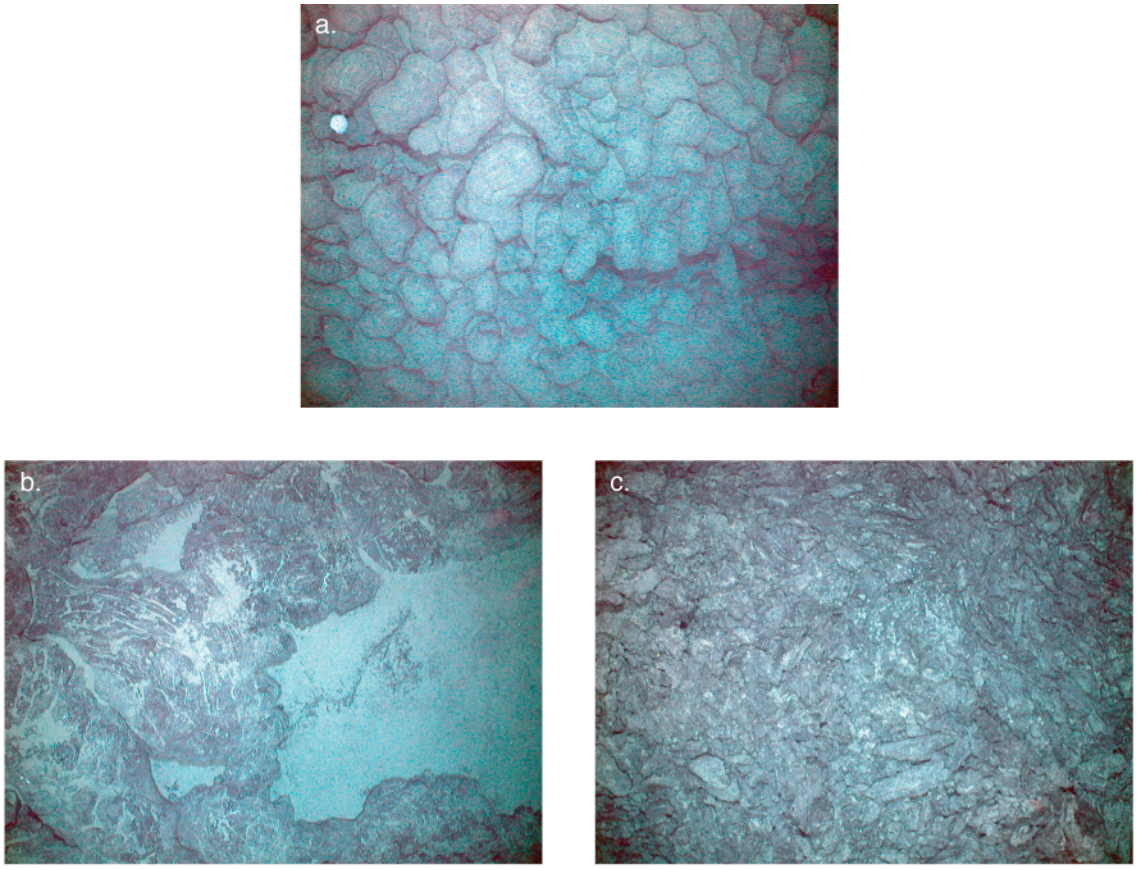

Figure 5. Three camera-tow images showing the classification of volcanic morphologies. a. Pillow flows appear as conglomerates of volcanic mounds, but they can also be cylindrical. b. Surficially, lobate flows are similar to pillow mounds but tend to be more amorphous. c. Sheet flows usually have the hackly texture that is pictured but can also be smooth and ropy.

Sheet flows are prevalent at fast-spreading ridges and in areas with low-viscosity magma. Fast-spreading ridges are generally associated with steady, robust magma sources that cause effusion to be relatively high. Lobate flows are midway between pillows and sheets on the morphology spectrum. This morphology is associated with an intermediate rate of effusion. Like pillow flows, lobates progress one lobe at a time, but they are erupted quickly enough that the lobes can amalgamate in a fashion similar to sheets.

Results

Based on the determination of flow boundaries from the sidescan sonar and image analysis, I composed a geologic map of the median valley floor, indicating the volcanic morphology and sediment cover of each flow area (Fig. 6). In areas where the TowCam did not transect flow areas, morphology and sediment cover were inferred from areas where images had been obtained.

According to sediment classification, the oldest flows (completely sedimented and mostly sediment areas) are concentrated at the west and east edge of the survey area. This distribution follows our general expectation that the ages of flows increase with distance from the axis. In the west, the oldest flows (completely sedimented) are concentrated around the northwest ridge on the seamount platform. In the east, the oldest flows are located on the northeast flank of the summit cones and along the perimeter of the seamount platform. There is no apparent pattern of distribution for high-sediment flows: they are widespread on both sides of the accretionary axis.

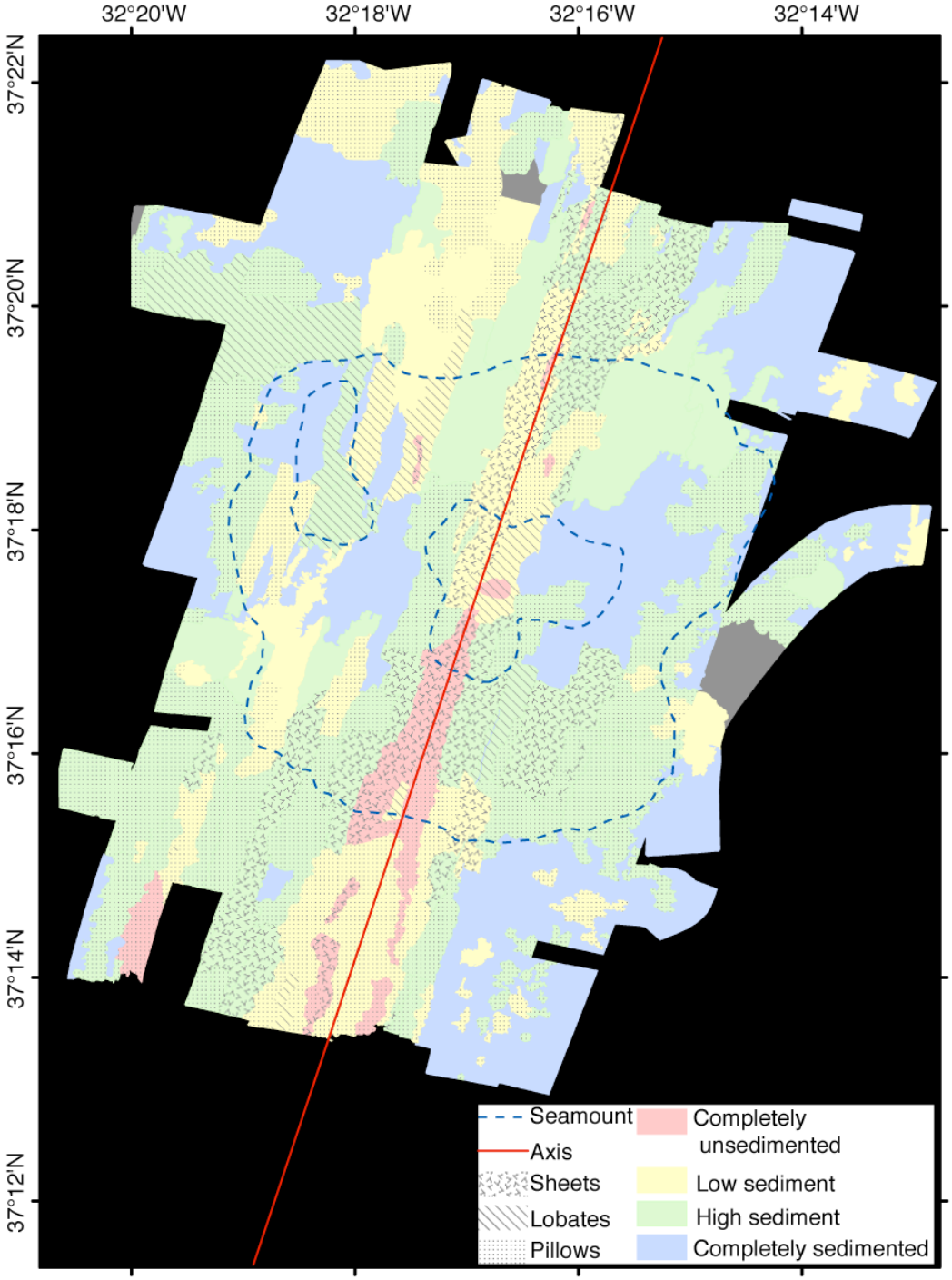

Figure 6. Geologic interpretation of the survey area based on sidescan textures and overlying seafloor photographs. Color indicates sediment cover level, and hatch marks indicate volcanic morphology type.

Low-sediment flows are emplaced in two parallel bands—the first is located along the inferred current axis of accretion, and the second is parallel to and west of the axis. Both bands are confined by two inner axial grabens (referring to two grabens within the larger axial graben structure, which were also identified by Singh et al. (2006)). The area of young, completely unsedimented flows is relatively small and is concentrated in a narrow band (<1,100 m wide) around the inferred axis. The young flows within the summit cones make up the lava lake. Young flows north of the lava lake are intermittent. Most young flows are found in a band south of the seamount, although a massive pillow flow in the southwest indicates recent off-axis volcanic construction.

The emplacement of volcanic morphologies also relates to bathymetric features and the axis. Pillows are unsurprisingly found in abundance throughout the study area. The majority of the pillow lavas are found at or beyond the perimeter of the seamount base, including the young off-axis pillow hummocks in the southwest. The location of low-lying pillow flows is restricted mainly to the seamount platform. Lobate flows are concentrated dominantly in the northwest quadrant of the seamount platform; they correspond to the location of a topographic high, the north-trending northwest seamount ridge. Smaller areas of lobate flows also occur intermittently along the accretionary axis. Sheet flows are predominantly confined to a 1000-2000 m band around the accretionary axis. Sheets that are located outside the accretionary zone were emplaced as flow bands (high length-to-width ratio) whose lengthwise aspects are axis-parallel.

Implications of Volcanic Morphology Distribution

The location of pillow, lobate, and sheet flows relative to the axis and magma chamber are also useful in characterizing the accretion system at Lucky Strike.

Observations on a global scale have concluded that slow-spreading ridges are dominated by pillow flows and fast-spreading ridges are dominated by sheet flows (Perfit and Chadwick, 1998). However, the location of pillows and sheets on a segment scale is integral to understanding the magmatic processes that affect Lucky Strike as an individual ridge.

In general (at all spreading ridges), sheet flows dominate the axial area (directly above the magma source) and topographic highs of segments, while pillows are prevalent in distal areas where effusion rates are low (Kennish and Lutz, 1998). Lucky Strike follows this global pattern of volcanic morphology distribution.

VOLCANISM VERSUS SPREADING RATE

The distribution of volcanic morphology types within a single ridge segment can indicate local variations in magma supply. However, the extent to which a particular morphology type is observed often varies by spreading rate. By determining the proportions of the volcanic morphology types, I was able to quantitatively compare Lucky Strike's volcanic properties to those of other ridges with a range of spreading rates.

Methods

I grouped the images into bins according to latitude and distance from the axis—each bin represents a 500 m interval of a single camera tow (Fig. 7). The inferred axis runs through 32°18′W x 37°11′N and 32°15′W x 37°21′N, trending parallel to the bounding faults, and passing through the accretionary zone as determined by the location of the youngest flows. I used nine bins to the west of the axis (4500 m) and six bins to the east (3000 m). The proportion of pillows, lobates, sheets was determined using the frame-by-frame classifications of morphology.

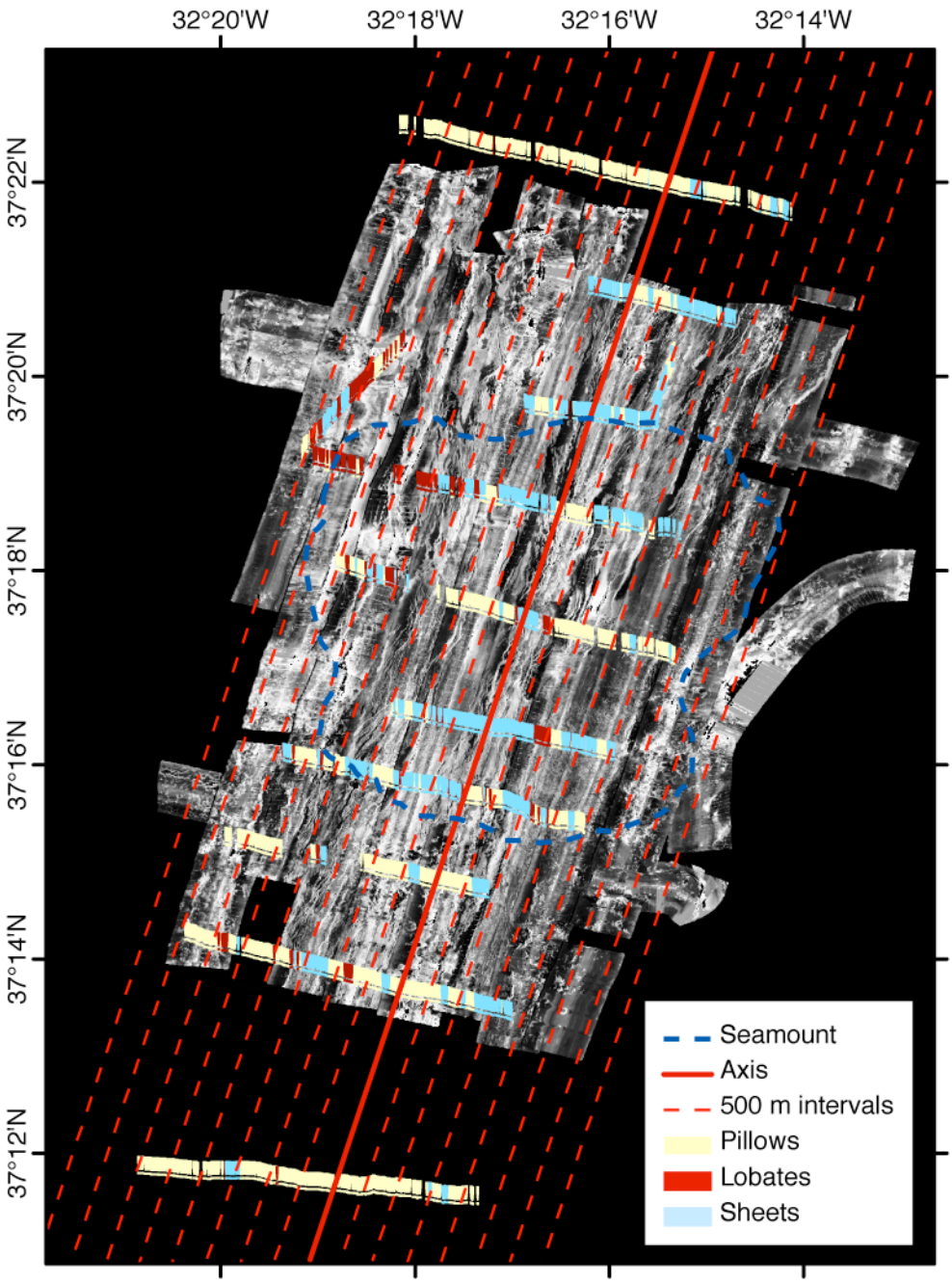

Figure 7. Distribution of volcanic morphology observations (using TowCam photos) relative to bin intervals. Each image location is marked by color according to its morphology type. The thick red line is the inferred accretionary axis, and the dashed red lines are the 500-m bin markers. Morphology is also shown relative to the seamount, the blue dashed line.

Results

I determined the along-axis (Fig. 8; Table 1) and across-axis (Fig. 9; Table 2) distribution. This allowed me to quantify the (geographic) pattern observations we made above. Subsequently, I was able to calculate the total proportion of sheet, lobate, and pillow flows, and also to determine the distribution with respect to the axis and seamount (Table 3). In total, the relative distribution of volcanic morphologies identified from the images in the study area is 57.6% pillows, 9.5% lobates, and 32.9% sheets. The on-axis flows are defined as the bins within 500 m of the inferred axis line; likewise, off-axis flows are all bins more than 500 m away.

Implications of Proportions of Volcanic Morphology Types

While the geographic distribution of volcanic morphology types is normal at Lucky Strike, quantitative analysis of sheet-pillow ratios indicates a continuous, robust magma chamber that may not be considered typical for a slow-spreading ridge. Studies of spreading ridges with various spreading rates show that the dominant morphology at a given segment is a function of the full spreading rate (Bonatti and Harrison, 1988; Perfit and Chadwick, 1998). As the full spreading rate increases, the percentage of sheets (determined aerially in previous studies) also increases. Bonatti and Harrison (1988) estimated the distribution to be 5-15% sheets and 85-95% pillows for the Mid-Atlantic Ridge, 37°N. This contrasts with my estimate of ~ 36.3% sheets to 64.7% pillows at Lucky Strike (Fig. 10), which is more comparable to estimates on the fast-spreading East Pacific Rise 12°50′N (Perfit and Chadwick, 1998)(110 mm/yr spreading rate) (McClain et al., 1985).

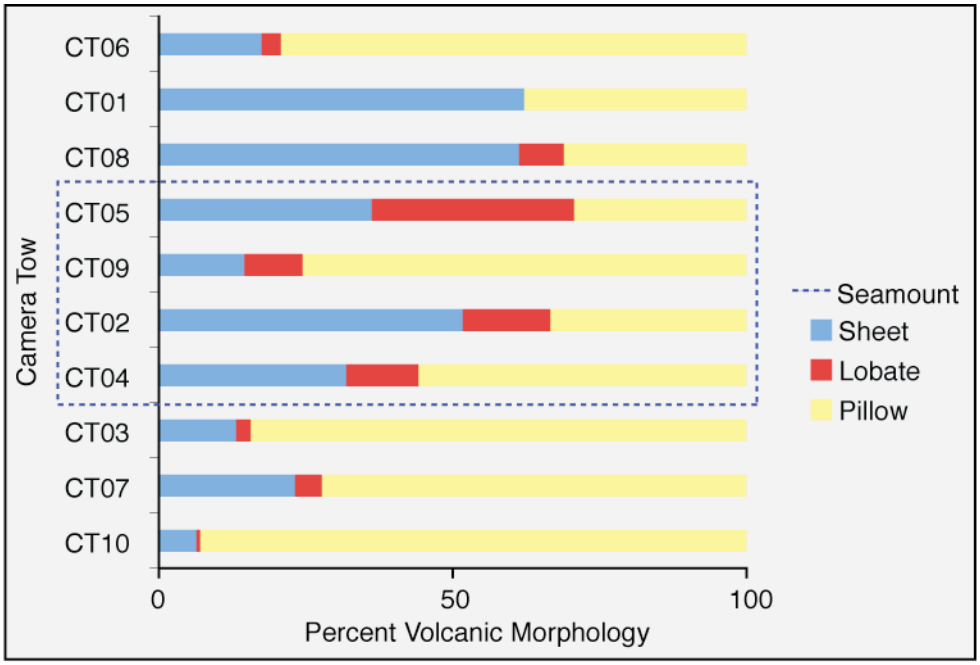

Figure 8. Along-axis distribution of sheet, lobate, and pillow flows by camera tow.

TABLE 1. ALONG-AXIS DISTRIBUTION OF VOLCANIC MORPHOLOGY TYPES

Track Number	Latitude (Decimal degrees)	Sheet (%)	Lobate (%)	Pillow (%)
CT06	37.37	17.5	3.2	79.2
CT01	37.35	62.2	0.0	37.8
CT08	37.33	61.3	7.6	31.0
CT05	37.31	32.4	36.5	31.1
CT09	37.29	14.6	9.9	75.4
CT02	37.27	51.7	14.9	33.3
CT04	37.26	31.9	12.3	55.8
CT03	37.25	13.1	2.6	84.3
CT07	37.23	23.2	4.6	72.2
CT10	37.19	6.4	0.7	92.9

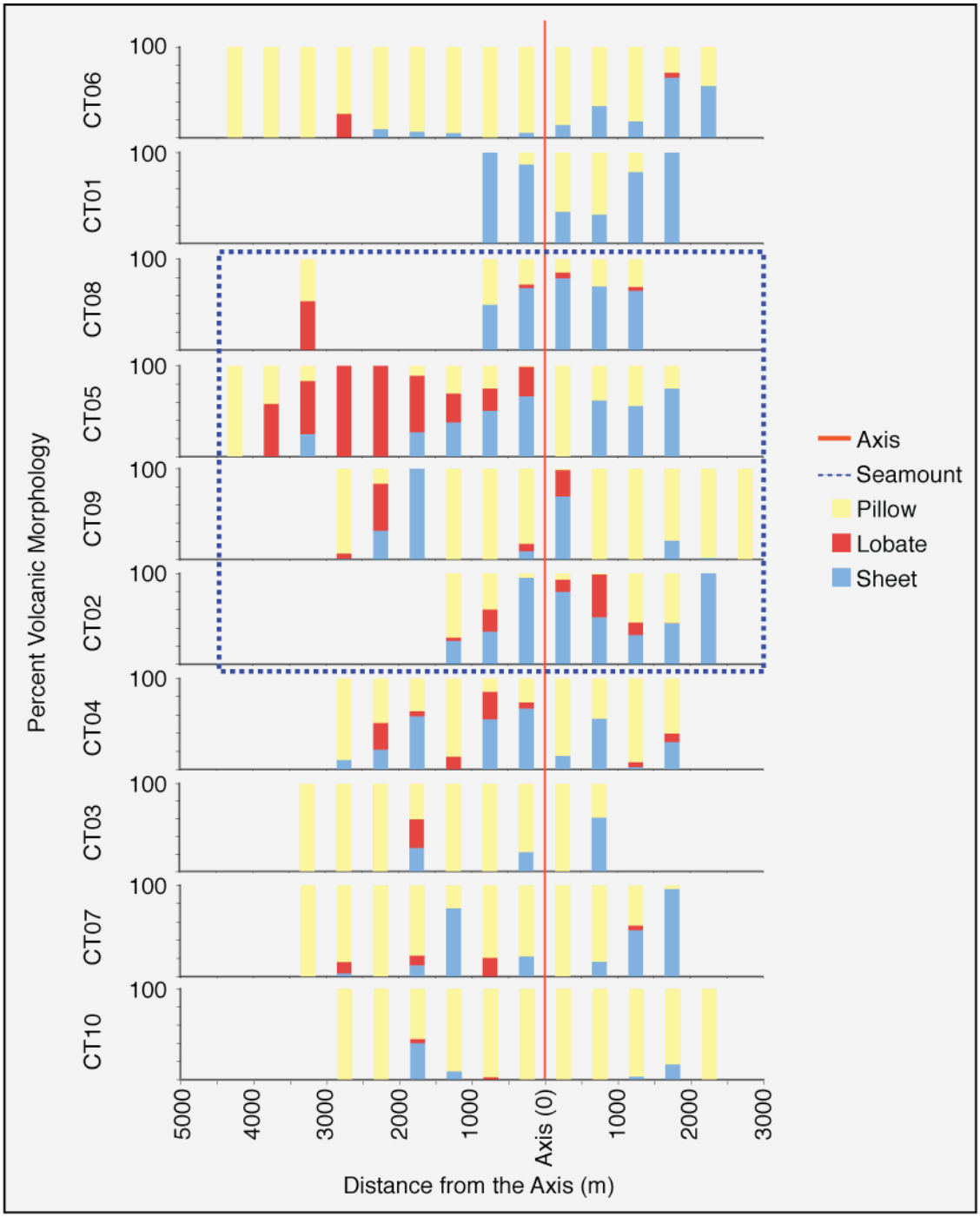

Figure 9. Across-axis distribution of sheet, lobate, and pillow flows by camera tow number. Each interval represents the distribution for a 500-m interval on one tow line.

TABLE 2. ACROSS-AXIS DISTRIBUTION OF VOLCANIC MORPHOLOGY TYPES

Distance from the Axis (m)	Direction from the Axis (m)	Sheet (%)	Lobate (%)	Pillow (%)
4500-4000	West	0.0	0.0	100.0
4000-3500	West	0.0	43.7	69.6
3500-3000	West	10.6	34.2	55.2
3000-2500	West	3.5	7.2	89.3
2500-2000	West	12.9	20.5	66.7
2000-1500	West	35.1	11.7	53.2
1500-1000	West	23.8	7.8	68.4
1000-500	West	25.5	14.4	60.2
500-0	West	47.4	4.2	48.4
0-500	East	33.2	5.7	61.1
500-1000	East	38.7	8.5	52.8
1000-1500	East	49.8	4.9	45.2
1500-2000	East	52.5	1.8	45.8
2000-2500	East	12.8	0.0	87.2
2500-3000	East	0.0	0.0	100.0

TABLE 3. TOTAL VOLCANIC MORPHOLOGY DISTRIBUTION

	Sheet (%)	Lobate (%)	Pillow (%)
Total	32.9	9.5	57.6
On-Axis	40.4	4.9	54.7
Off-Axis	30.9	10.7	58.4
On-Seamount	43.4	14.5	42.1
Off-Seamount	23.8	5.1	71.0

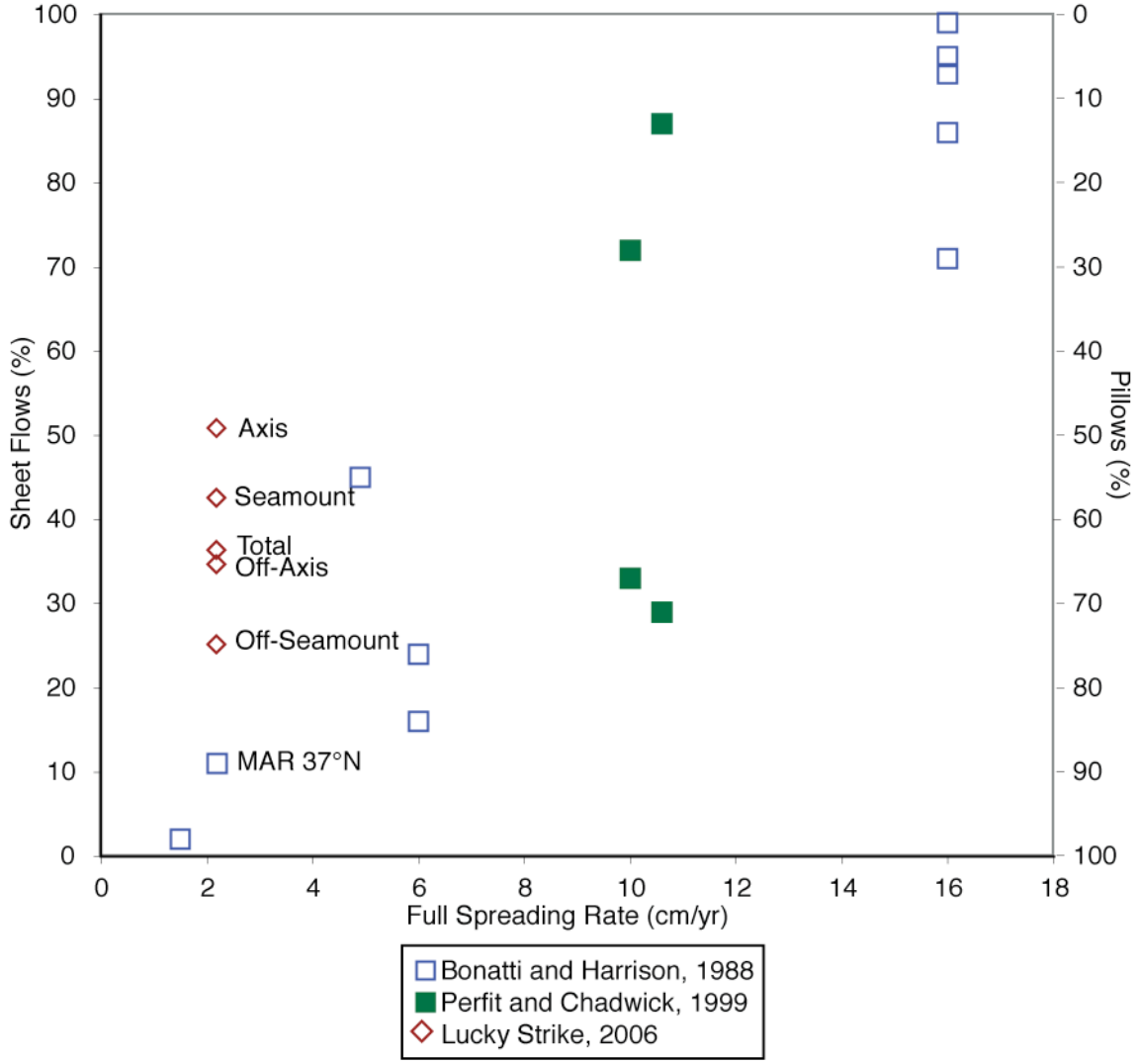

Figure 10. Modified and expanded from Bonatti and Harrison (1988) and Perfit and Chadwick (1998). Proportion of sheet flows as a function of spreading rate. Generally, a higher percentage of sheet flows is observed at fast-spreading ridges. Open boxes show sheet-to-pillow ratio determined in our study compared to the global trend. Note that ratios determined for the total and off-axis, on-axis, off-seamount and on-seamount areas are all higher than generally observed for the nearby MAR 37ºN.

As the aforementioned studies on spreading rate versus volcanic morphology do not account for the presence of lobate flows, our estimate removes the proportion of lobates observed at Lucky Strike for comparison (Table 4). Note that the sheet-to-pillow ratio was determined using the camera tow images, not by areal distribution as in the previous 1988 and 1998 studies. As the TowCam data set is quite expansive (>16, 000 photos) and covers across-axis transects over a 16 m-long area, we consider our values an accurate estimate of the distribution of morphology types. Furthermore, our camera tow data covers a small area at the center of the segment, where we would expect a higher proportion of sheet flows, owing to the influences on magmatism by the axial magma chamber and central magma focusing. However, off-seamount (25.1% sheets: 74.9% pillows) and off-axis (34.6% sheets: 65.4% pillows) volcanic emplacent still show an abundance of sheet flows compared to the values estimated by Bonatti and Harrison (1988). These results possibly indicate that the pattern of morphology distribution is not only a result of magma focusing, but of a robust magma supply affecting the whole inner rift valley.

TABLE 4. TOTAL VOLCANIC MORPHOLOGY DISTRIBUTION (EXCLUDES LOBATE FLOWS)

	Sheet (%)	Pillow (%)
Total	36.3	63.7
On-Axis	42.5	57.5
Off-Axis	34.6	65.4
On-Seamount	50.8	49.2
Off-Seamount	25.1	74.9

Note: These ratios were used to compare the distribution of morphology types at Lucky Strike to the global trend (Figure 15).

Although Lucky Strike is a slow-spreading ridge, it exhibits lava emplacement properties typical of its fast-spreading counterparts. The Azores hotspot is thought to be the main contributor to the segment's relatively high magma budget. The high proportion of sheet flows indicate a high magma effusion rate that is commonly associated with a continuous magma supply not typically found at slow-spreading ridges. Other physical expressions of a robust magma supply are the on-axis seamount, lava lake, and hydrothermal field—features that would require a continuous source of magma and heat. The construction and perpetuation (the lava lake is young, and the hydrothermal field is still active) of the structures is particularly remarkable, given that the axial magma chamber is twice the depth of magma chambers found at fast-spreading ridges.

The widespread magmatic influence of the axial magma chamber is also notable, as it is only 3-4 km wide and 7 km along axis, but contributes to construction of a seamount (6 km wide and 8 km long) twice its width. The waning influence of the high magma supply is observed at the perimeter of the seamount base, with the increase in pillow flows. Here, the local magma budget is lower than above the axial magma chamber, and the effusion rate is necessarily slower, resulting in the change of morphology. We consider two possibilities for the systematic appearance of these pillow flows. In the first case, these distal flows are erupted through dikes that propagate laterally from the axial magma chamber. Alternatively, these flows are emplaced by smaller, isolated melt sources that are unrelated to the primary axial magma source. Future analysis of the trace and rare earth element geochemistry could determine whether these distal flows originate from the same magma source as on-seamount flows or from smaller, isolated melt zones.

Data from the 3-D seismic survey (Singh et al., 2006) show that the melt lens of the axial magma chamber shallows slightly from north to south. We believe that this contributes to the concentration of young flows to the south of the summit cones. Furthermore, the axial magma chamber does not extend as far to the south as to the north, relative to our study area. An increased distance from the magma source, which would require greater dike propagation lengths in order to emplace lava beyond the seamount, thus contributes to the high density of hummocks to the south of the seamount, compared to the north.

FAULTING

Methods

Fault Identification Using TowCam Data

Fault scarps are mapped by using the sidescan images to identify linear features with high backscatter, but resolution of the sidescan makes measuring vertical offset difficult. Additionally, the northernmost and southernmost camera tows (CT06 and CT10, respectively) do not overlap with the sidescan images. Using the seafloor photos as opposed to the sidescan allowed me to interpolate the results of fault analysis over a slightly larger area; I am thus able to identify smaller fault scarps that are not otherwise recorded on the sidescan due to missing data and the variable topography associated with slow-spreading ridges (e.g. Fig. 11).

For each scarp I measured fault heave (*h)*, or horizontal offset, using the camera tow images by recording the distance between two photos, one containing the fault line and one containing the top-most edge of the fault scarp. The error of *h* is approximately 4 m, equivalent to the width of one photograph frame.

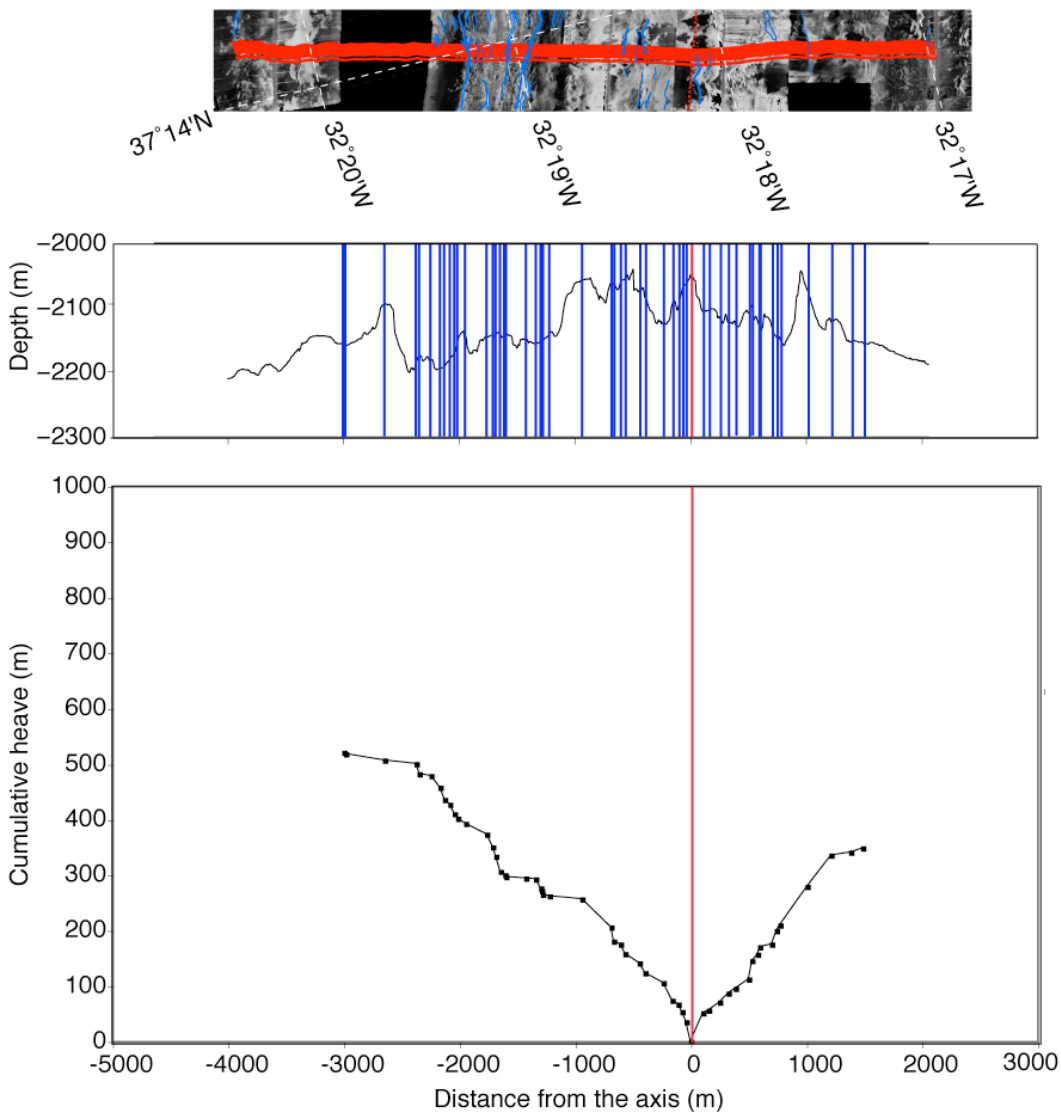

Figure 11. Sidescan image, bathymetric profile, and cumulative heave plot of CT07 (southern camera tow). Faults are marked in blue. The thin vertical line is the inferred accretionary axis. The thick red line (on sidescan only) shows the camera tow line. Note the difference between faults mapped in the sidescan and faults identified in the camera tows. Using the seafloor photos, we observe smaller faults that are not imaged on the sidescan; additionally, we observe faults in areas where sidescan quality is low (i.e. in the nadir, seams, or in areas of missing data).

Measuring Tectonic Extension

Estimates of tectonic elongation (e) were calculated using the heave (h) and fault spacing (s) measurements determined through the camera tow images. We use three methods of calculating e, based on methods by Escartin et al. (1999). Note that the terms strain (ε) used by Escartin et al. (1999) and elongation (e) used in this study are synonymous. In the first method,

$$e = \text{mean } h / \text{mean } s, \quad (1)$$

where s denotes the distance between the centers of two adjacent faults. In the second method,

$$e = \Sigma h / L, \quad (2)$$

where L represents the length (m) of the transect, in this case the portion of the camera tow overlain with faults. For the third method,

$$e = m, \quad (3)$$

the slopes of the cumulative heave plot.

Results

The sidescan images indicate that the axial valley is characterized by axis-parallel faults (Fig. 12). The majority of faulting is found within 4000 m west and 2500 m east of the accretionary axis. The across-axis width of the active faulting zone widens northward, from 5000 m to 7000 m. The most prominent tectonic feature is a 4000 m-wide graben whose faults overlie the northwest ridge and the summit cones. Faulting within this graben has formed two ‘inner graben’ structures, as well.

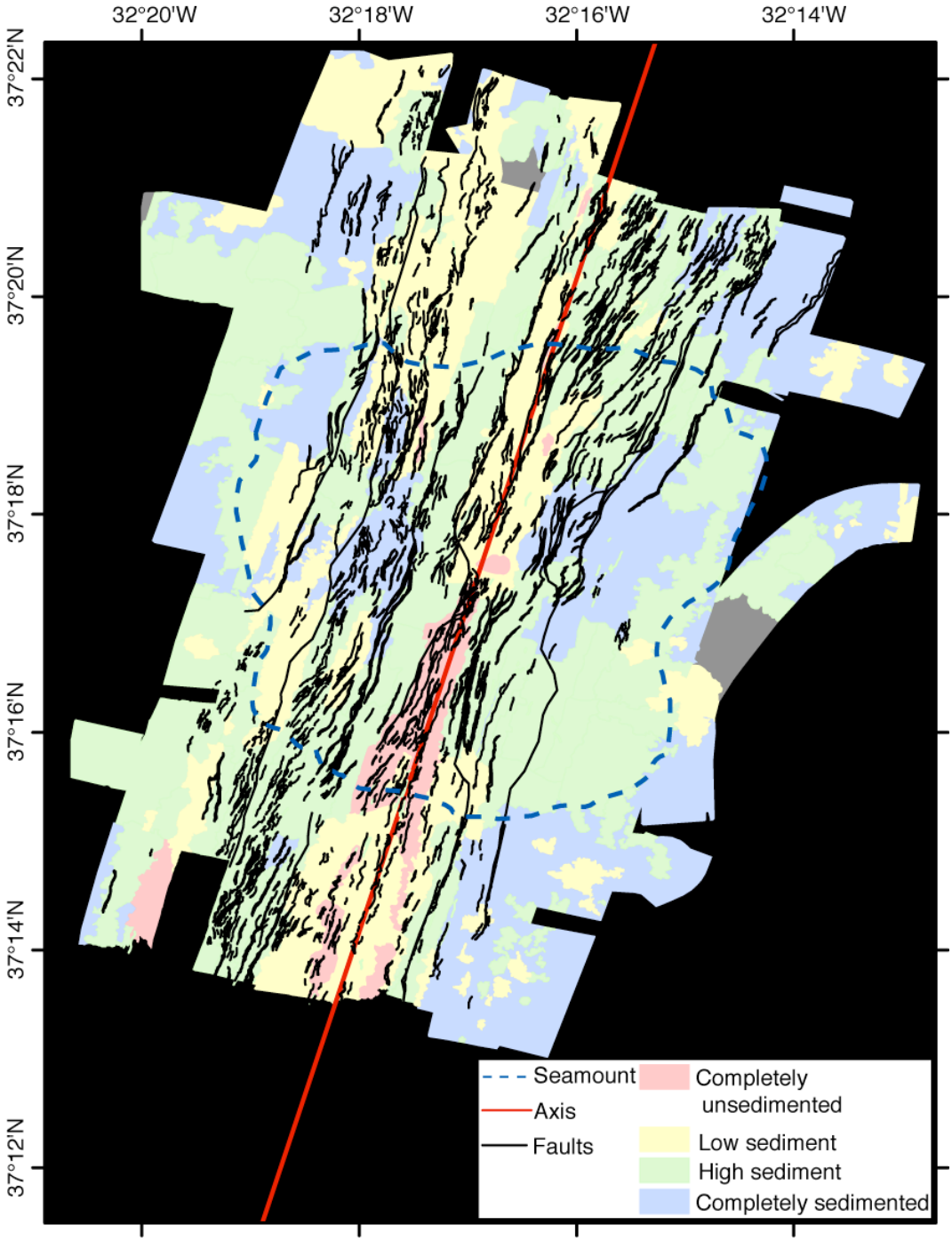

Figure 12. Interpretation of sediment cover, inferring relative age, with respect to fault fabric (modified and expanded from Escartin, unpublished). Younger flows will have less sediment cover.

Based on all three measures, tectonic elongation accounts for 19% of across-axis horizontal extension. The amount of tectonic elongation is equal on both sides, with 19±2% extension accumulation to the east of the axis, and 19±3% extension accumulation to the west (Fig. 13). The remaining 81% of horizontal extension is therefore taken up by magmatic accretion or ductile tectonic processes (Escartin et al., 1999). Along the strike of the volcanic axis, tectonic elongation remains constant, with the exception of CT02, which shows a low elongation estimate of 9.7% (Fig. 14). This low elongation value is likely a cause of the younger flows paving over faults, and also the untectonized zones on either side of the axis.

Terrestrial fault studies have estimated extension from "small," unsampled faults to determine total elongation (e.g. Marrett and Allmendinger, 1992; Gross and Engelder, 1995). An individual small fault (meter to decimeter scale) would account for an insignificant fraction of elongation, but numerous unsampled small faults would result in a deficient estimate of elongation. This is especially relevant to seafloor studies, where data collection is limited by resolution of sidescan sonar data and to the areas covered by tow cameras and submersibles. Total elongation in a region can be inferred from the heave for each fault and the cumulative number of faults sampled (N). The number of faults with displacement greater than or equal to *d* is written as

$$N \approx d^{-C}, \qquad (4)$$

where C characterizes the relative number of large faults to small faults. C is the negative slope of the central, linear portion of a log N vs. log *h* plot. Total elongation can be estimated using *N* and C<1.

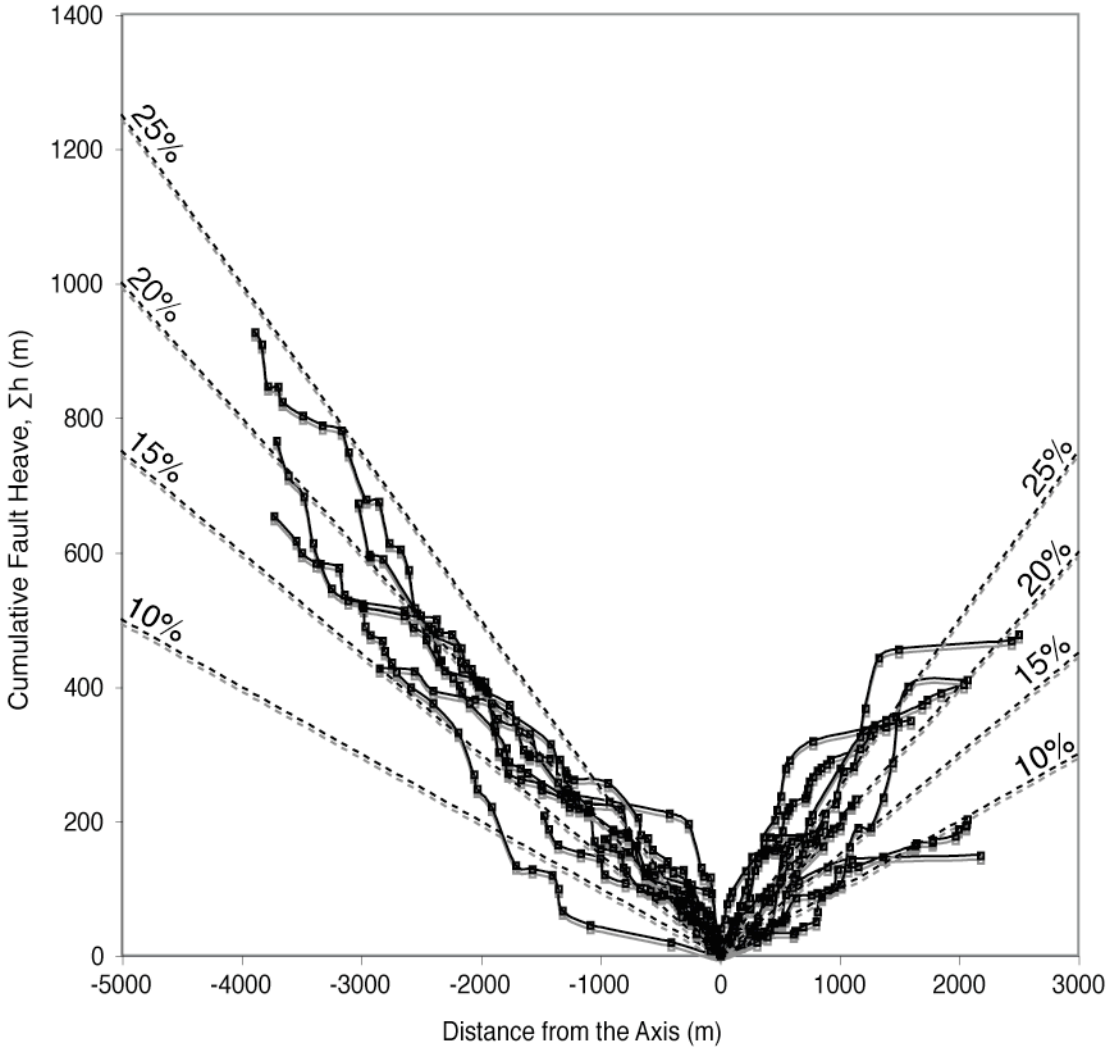

Figure 13. Plot of cumulative fault heave (∑h) versus distance from the inferred axis for faults observed in the 10 across axis camera tows. Negative distances are west of the axis. The dashed lines are the 10%, 15%, 20%, and 25% strain markers, shown for reference.

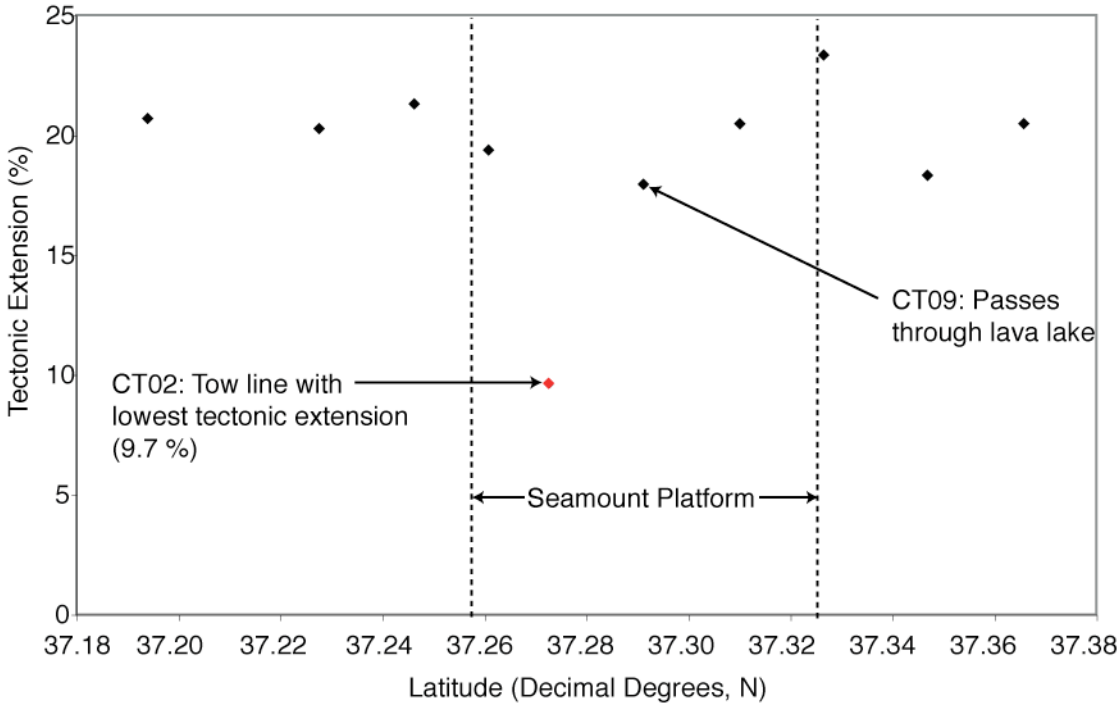

Figure 14. Along-axis graph of tectonic extension. There is little variability in tectonic elongation along-axis, except at CT02 (south of the summit cones). This is likely a result of the west and east zones of untectonized seafloor on either side of the axial area, where very little faulting occurs.

The fault displacement population for Lucky Strike (Fig. 15) includes the fault number and respective heave for all faults sampled in the camera tows. C≈1.58, indicating that elongation due to small faults is more than or equal to the elongation due to large faults. Therefore, the 19% tectonic elongation estimate is significantly less than the true value, which cannot accurately be estimated from the sampled population of faults.

Implications of Estimates of Tectonic Elongation

Faults nucleate within the axial valley and tend to have narrow spacing (Escartin et al., 1999; Behn et al., 2002) and small heave lengths. However, relative to fast-spreading counterparts, slow-spreading ridges are characterized by faults that are longer and have greater heaves (Behn et al., 2002). Because volcanism is intermittent, faults in slow-spreading ridges are not continually paved over by new eruptions, allowing for both along-strike and along-dip growth of fault scarps. Lateral growth of faults is often accommodated by fault linkage (Alexander and MacDonald, 1996; Escartin et al., 1999). Additionally, fault surfaces can be reactivated and develop larger heaves when they reach the rift valley walls (east and west bounding faults) (Escartin et al., 1999).

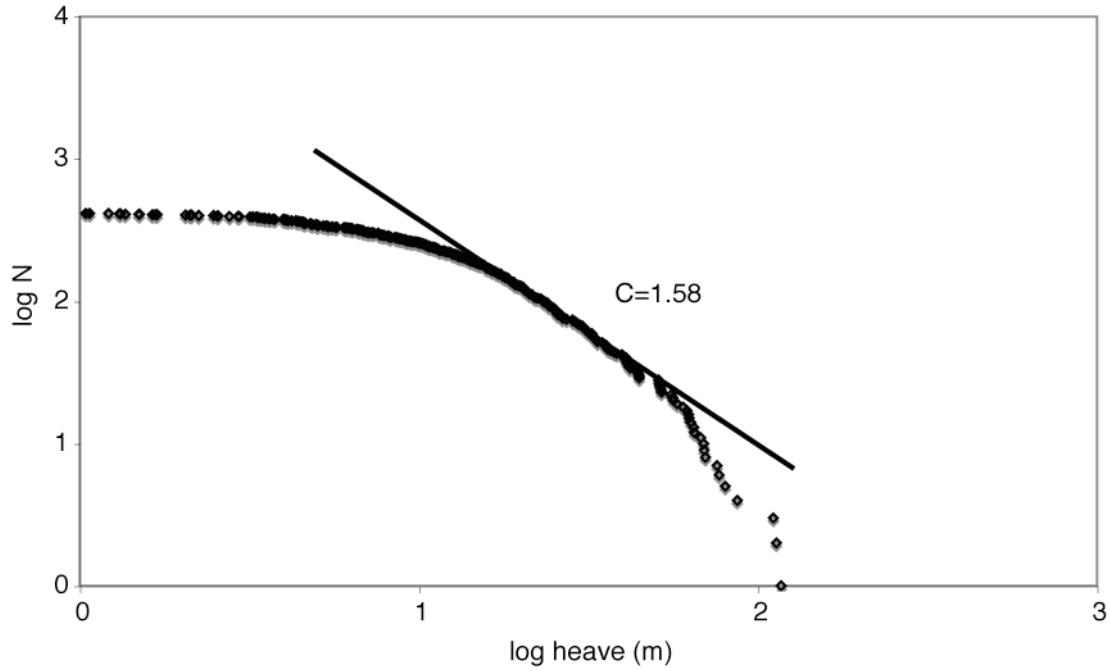

Figure 15. Fault displacement population of all faults identified through the camera tow images. C=1.58, indicating that the 19% elongation value underestimates the true elongation value for the survey area.

The widths of active fault zones (i.e. the along-axis range over which fault heave can continue to increase) vary by ridge segment, but tend to extend between 8-12 km from the axis (Searle et al., 1998) along the MAR. Lucky Strike's faulting zone is much narrower (~4.5 km), with faulting localized over the segment's magma source. Based purely on quantitative analysis (>19% extension in the east and west), we would expect symmetric faulting about the axis. That is, similar values of extension should be accommodated by similar numbers of faults, over a symmetric faulting fabric. However, when comparing cumulative heave profiles of off-seamount (Fig. 16a) and on-seamount (Fig. 16b) camera tow track lines we recognize distinct differences in the style of extension accommodation between areas west and east of the axis. Cumulative heave profiles for off-seamount track lines are linear both west and east of the axis: the proportion of extension accommodated by faulting over a given distance remains constant.

In contrast, cumulative heave profiles of camera towlines over the seamount indicate that extension accumulation is localized closer to the axis. Both sidescan sonar imaging and seafloor photos indicate a 700-1300 m wide zone of highly tectonized seafloor over the axis. East of this zone, tectonic extension becomes insignificant; the few faults located east of the highly tectonized axis region have small heaves (5-30 m) and therefore contribute little to cumulative extension. West of the tectonized axis region lies another unfaulted zone (600-1000 m wide), beyond which faulting exhibits a linear accumulation of extension (similar to off-seamount extension).

This comparison indicates that the style of tectonic extension over the seamount is more variable than in areas beyond the seamount platform. The seamount is the surface

expression of anomalous magmatic influence by the axial magma chamber (i.e. beyond the perimeter of the seamount, the ridge segment appears to behave much like a typical slow-spreading ridge); this implies a relationship between the presences of an active, robust magma source and the variability in extension accumulation over the seamount. A fast-spreading ridge study suggests that localized fault growth and strain accumulation (asymmetric fault distribution) is possible over short time periods (Escartin et al., 2007) but becomes symmetrical with time (and presumably distance from the axis).

Localization of tectonic extension at the axis is therefore not necessarily unusual. Factors that might contribute to such localization are repavement of faults by previous eruptions during a period of intense volcanism (subsequently removing any evidence at the surface of faulting) and local variations in crustal thickness. Thick, brittle crust is more likely to accommodate faulting than thinner crustal regions.

The minimum tectonic elongation estimates for Lucky Strike are far greater than those estimated for the neighboring FAMOUS segment. Estimates for the valley floor are 4% and 6% elongation for the west and east, respectively (MacDonald and Luyendyk, 1977). However, Luyendyk and MacDonald (1977) further note that volcanism dominates the floor, and faults are only 2-10 m in heave height. As Lucky Strike is heavily faulted, and faults overprint the newest eruptions, a higher tectonic elongation estimate is to be expected.

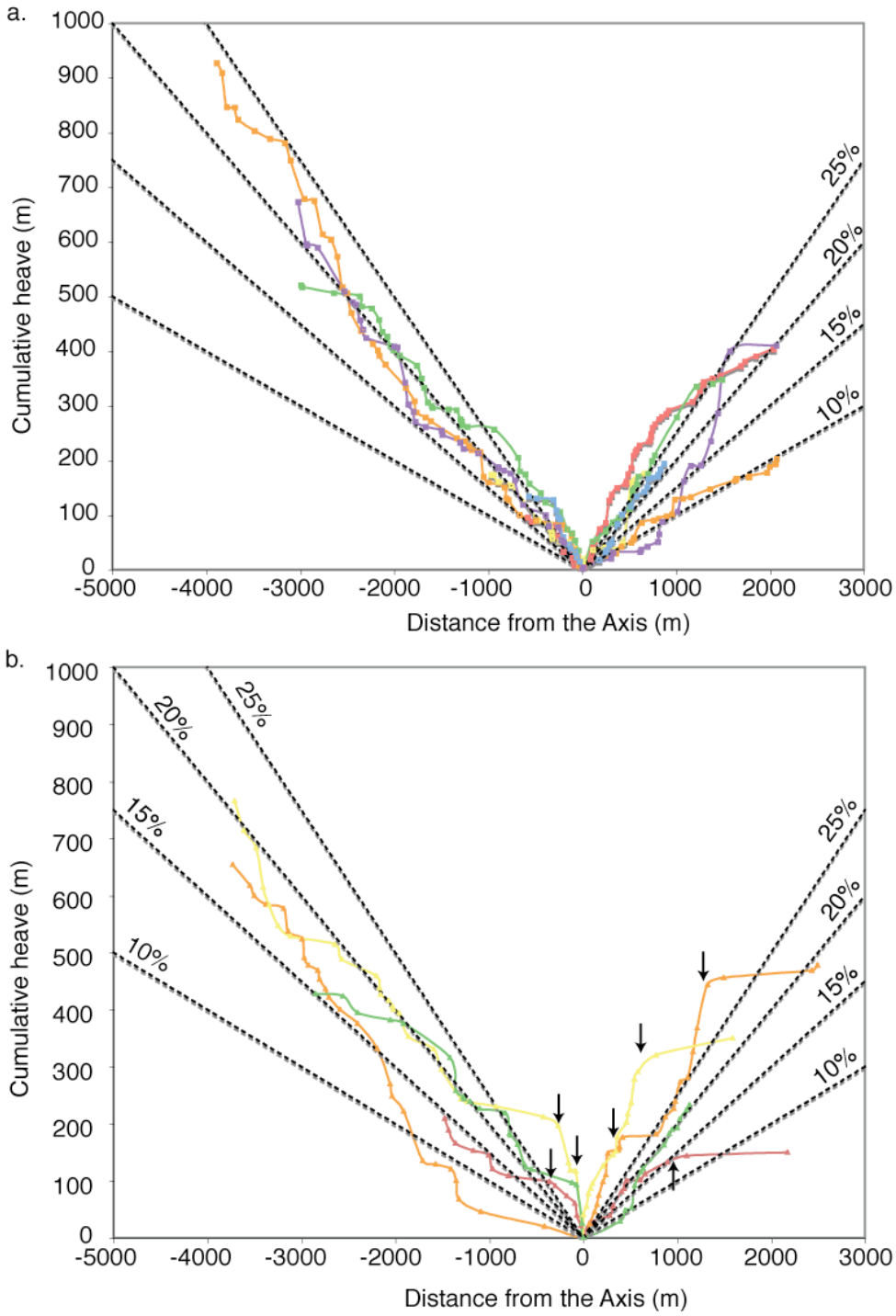

Figure 16. a. Cumulative heave plot of off-seamount tracklines. b. Cumulative heave plots of over-seamount tracklines. Dashed lines indicate the 25%, 20%, 15% and 10% extension markers. Arrows indicate the distance at which significant surface tectonism ceases, causing accomodation of extension by faults to end.

DISCUSSION

Geologic History of the Study Area

The multibeam bathymetry and sidescan sonar data, supplemented by analysis of the seafloor photographs, provide the means for reconstructing a relative timeline of the formation of features within the Lucky Strike rift valley. Based on the 11 km rift valley width and full spreading rate of 22 mm/yr, the area within the valley represents 500-550 kyr of spreading; all features within the rift, including formation of the bounding faults, must therefore have formed within the past 500-550 kyr. Following the formation of the axial valley is the construction of the seamount platform, and subsequently the formation of the northwest ridge and three summit cones. The ridge and summit cones would have occurred within a similar time frame, considering that both are overprinted with high to complete sediment cover. The multibeam bathymetry and sidescan both show that the axial graben faults cut through the ridge and summit cones, indicating that the faults nucleated after seamount construction. Additionally, the low-sediment flows are constrained by the two axial grabens in on-axis and axis- parallel bands; eruption of these flows must have been syn- or post-tectonic.

The youngest flows are concentrated south of the summit cones, with the exception of the formation of a young volcanic pillow ridge in the southwest corner of the study area. The confinement of these young flows to the graben structures, and their subsequent faulting, indicate that the segment undergoes periodic episodes of tectonic and volcanic dominance. The youngest feature in our study area is most likely the lava lake, which overprints faults through the seamount summit cones.

Using estimates of sediment thickness from the images, age brackets were assigned to the series of events described above (Fig. 17). Sediment accumulation rates have been estimated at 2.9 cm/kyr (Nozaki et al., 1977) and 2.7-3.7 cm/kyr (Cave et al., 2001) for two nearby segments. For our calculations we use a sedimentation rate of 3 cm/kyr and an average seafloor roughness of 1 m: it would require an average 1 m of vertical sediment accumulation to completely cover volcanic features of the seafloor. Given these assumptions, I estimated sediment thickness for each of the four classifications of sediment level: areas with bare rock have <10 cm, low-sediment regions have 10-60 cm, high-sediment regions have 60-100 cm, and completely sedimented areas have >100 cm of sediment cover. Based on the sedimentation rate of 3 cm/kyr, the estimated thicknesses correspond to approximate ages of <3 kyr, 3-20 kyr, 20-33 kyr, and >33 kyr. The eastern flanks of the northwest seamount ridge and summit cones are completely sedimented, although the majority of the seamount platform and a considerable proportion of the surrounding pillow flows are observed to be highly sedimented. This indicates construction of the seamount, northwest ridge, and summit cones ended between 20-33 ka. Faulting of the seamount and formation of the axial graben occurred after the ridge and summit cones were formed. Low-sediment areas confined by the graben correlate to flows emplaced 3-20 ka. The most recent flows, the southwest pillow ridge and axial flows, were erupted less than 3 ka.

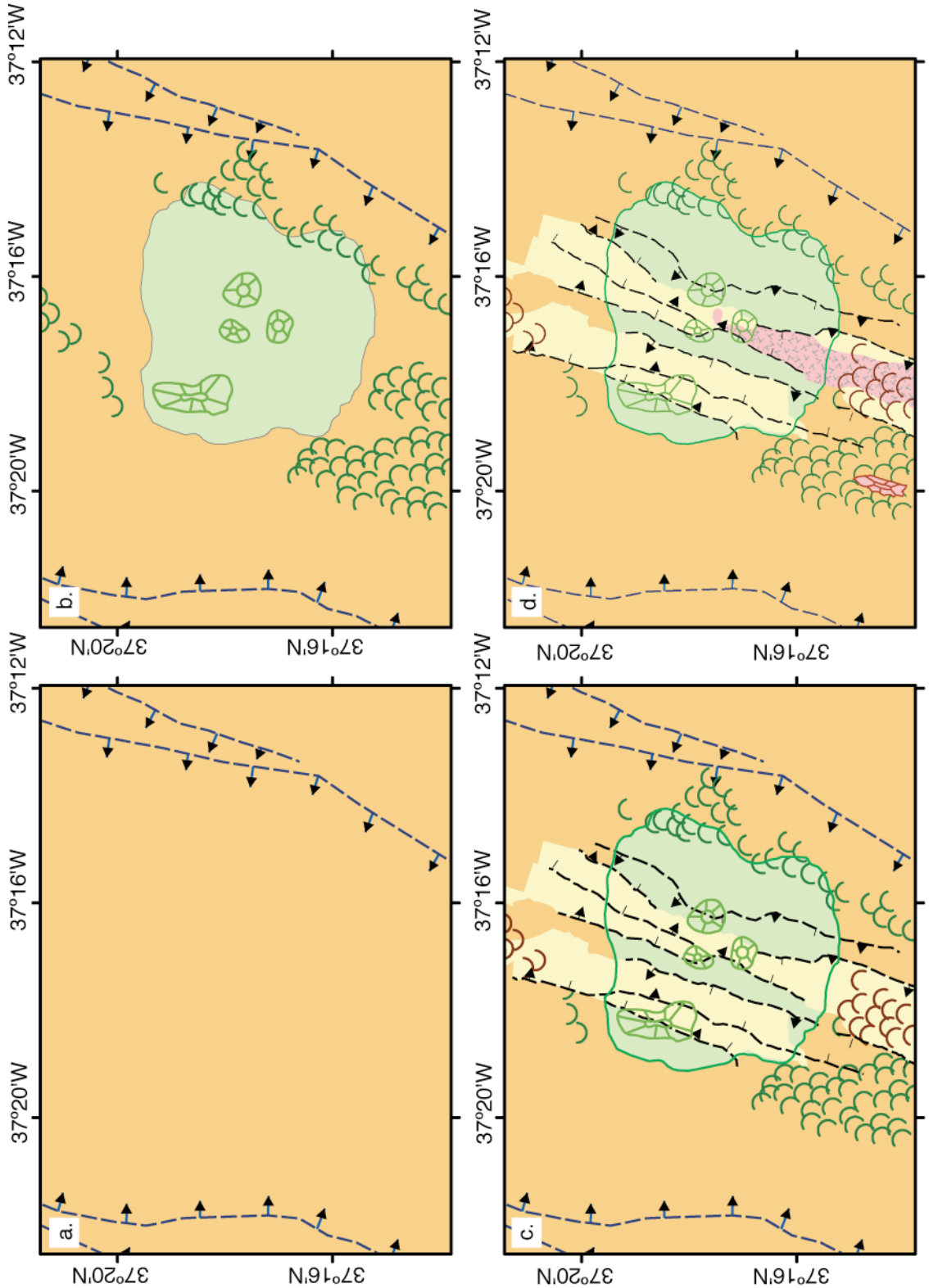
a.
b.
c.
d.
37°20'W
37°16'W
37°12'W
37°16'N
37°20'N

Figure 17. Four-panel reconstruction of the geologic history of Lucky Strike. a. Formation of the rift valley, contained by the west and east bounding faults. b. Formation of the seamount, northwest ridge, and summit cones ends 20-33 ka. Lava erupts as hummocky flows around seamount perimeter. c. Formation of grabens through the seamount. Continuing eruptions of distal hummocks. Syn- or post- tectonic eruption of flows within the graben (ends 3-20 ka). d. Sheet flows over the axis, formation of the lava lake, and off-axis eruptions characterize the most recent period of volcanism (within the last 3 kyr).

While seafloor images and the sediment rate are used to broadly determine local sediment thickness, it is difficult to estimate thickness beyond the decimeter scale. Our model for estimating sediment thickness assumes uniform distribution of sediment throughout the segment; below are potential factors contributing to non-uniform distribution of sediment and sediment redistribution that, given a more accurate sampling procedure (i.e. sub-bottom profiling), would have to be considered. Topographic features certainly result in areas that are preferential to sediment accumulation. The overall rough topography caused by extensive faulting at the segment center has led to the formation of grabens throughout the seafloor—these structures likely act as sediment traps. Additionally, upwelling of water above and around a topographic prominence (e.g. slopes of seamount, summit cones, volcanic ridges) prevent settling of fine sediment over these volcanic features (Lisitzin, 1972); relatively less sediment is deposited on the slope of an edifice than over its periphery. Sediment can be redistributed by means of ocean-bottom currents (e.g. Ruddiman, 1972). Previously documented seismic events at Lucky Strike (Dziak et al., 2004) also necessitates the consideration of seismic waves as a potential reorganizer of sediment (Lisitzin, 1972). Seismic waves cause bottom slides and roiling of sediment, resulting in resuspension.

Comparison to Other Ridges

Mapping and analysis of Lucky Strike, along with findings from previous research, has led to a more holistic and fine-scale understanding of the magmatic and tectonic processes at the segment. To fully comprehend the results of this study, it is necessary to view Lucky Strike in a general context, comparing the ridge to other slow-spreading segments.

The FAMOUS Segment

Project FAMOUS (French-American Mid-Ocean Undersea Study) has previously documented the volcanic morphology and tectonic evolution of the FAMOUS segment (35°50′-37°20′N) using acoustic surveys, large-area photography, sidescan sonar (Ramberg et al., 1977) and submersible *Alvin* dives (Ballard and Van Andel, 1977). As the segment lies south of Lucky Strike and is beyond the range of magmatic influence by the Azores hotspot, we will consider the FAMOUS segment as representative of slow-spreading MAR ridges for comparison.

Analysis of the area is given in individual dive summaries (Ballard and Van Andel, 1977), which makes comparison of volcanic morphology and eruption patterns between the Lucky Strike and FAMOUS segments difficult. Dive observations were used to characterize the volcanic construction features of the FAMOUS segment. The FAMOUS rift valley floor consists of volcanic hills 0.5-1 km wide, 2-4 km long, and 200-300 m height (Ramberg et al., 1977). These volcanic constructions represent a relatively intermittent magma system compared to Lucky Strike whose rift valley contains a 6-8 km wide, 400 m high seamount.

On a broader regional scale, the existence of a large central volcano on the axial valley floor of Lucky Strike is quite anomalous. More typically, MAR segments are characterized by an abundance of seamounts at the spreading axis. The density of seamounts over a given rift valley floor along the MAR has been projected at ~80 seamounts/1000 km^2 (Smith and Cann, 1990). Given this estimate we would expect to see 8-9 smaller seamounts in our study area, as opposed to the single large volcano observed. Seamounts along the MAR have a height range of 50-600 m (Smith and Cann,

1990), although the characteristic height of seamounts is 58 ±2 m (Magde and Smith, 1995).

The Reykjanes Ridge

The slow-spreading Reykjanes Ridge (MAR, 57°45′N) also serves as a worthy comparison for Lucky Strike. Reykjanes is also located near a hotspot, specifically ~1100 km from the center of the Iceland plume, although no increase in melt production is caused by this proximity (Sinha et al., 1998). Notably, it is the only other slow-spreading ridge for which a melt lens has been identified. The lens lies 2.5 km below the seafloor and is 4 km wide (Navin et al., 1998), similar in dimension to the axial magma chamber beneath Lucky Strike. Additionally, comparable crustal thicknesses have been reported for the two ridges: 6-7 km for Lucky Strike (Escartin et al., 2001) and 7-7.5 km for Reykjanes (Sinha et al., 1998). Overall, these factors indicate that the oceanic crust-building processes at the respective ridges should be similar.

Bouguer anomaly data has suggested that accretion follows a ridge-strike trend at Reykjanes (Pierce and Navin, 2002); this parallels the along-axis accretion pattern at Lucky Strike, exhibited by the young flows erupted length-wise along the axis. According to Reykjanes Ridge studies, the location of eruptions can be used to determine magma upwelling patterns. At fast-spreading ridges, magma is upwelled in a 2-D system, feeding volcanism along the length of the axis. Slow-spreading ridges are fed by 3-D upwelling systems which lead to central magma focusing, but more variable eruptions along axis (Pierce and Navin, 2002; Pierce et al., 2005). The latter system more accurately models Lucky Strike as the hydrothermal field, seamount, and location

of new axial flows signify central focusing. The youngest flows are confined to the small axial area over the seamount.

CONCLUSIONS

After detailed mapping of the area, I am able to make several observations regarding the surface expression of magmatic and tectonic processes influencing the Lucky Strike median valley:

1. The distribution of sheet, lobate, and pillow is consistent with other spreading ridges. The abundance of pillows increases with distance from the segment center (and magma source), and sheet flows are dominant in the axial region. Lobate flows are dominant over the northwest seamount ridge (however, this feature is ridge specific).
2. The sheet-to-pillow ratio (36.3 %: 63.7%) of Lucky Strike segment center is more typical of an intermediate- to fast-spreading ridges suggesting that the magma source feeding the region is more continuous than at other slow-spreading ridges.
3. The percent of extension accumulated by faulting is >19%. Magmatism and ductile tectonic processes accommodate the remaining percentage of extension.
4. The style of tectonic extension appears to be more variable over the seamount than in distal areas. The presence of an active, relatively robust magma source directly beneath the seamount likely contributes to this variability.
5. The relative geologic history of the area is as follows: formation of the axial valley occurred within the last 500-550 ka. This was followed by accretion of the seamount, including the northwest ridge and summit cones. Faulting of the seamount resulted in two parallel axial grabens. During or after activation of

these faults two parallel bands of flow were emplaced within the grabens. The most recent flows were accreted along the southern portion of the axis.

6. The youngest flows were accreted in the south in the form of a southwest pillow ridge, a narrow band of axial sheet flows, and a lava lake enclosed by the summit cones of the seamount. In terms of the whole segment, the most recent volcanism has dominated the center of the axial valley.

ACKNOWLEDGEMENTS

Thanks to Bereket Haileab (Carleton College), my comprehensive exercise advisor. Special thanks to the Woods Hole Oceanographic Institute Academic Programs office for all the help and support I received as a summer minority fellow. Finally, I wish to extend my deepest gratitude to Adam Soule, my advisor in Woods Hole. Thanks so much for your enthusiastic guidance and support throughout this project.

REFERENCES

Alexander, R. T., and MacDonald, K. C., 1996, Sea Beam, SeaMARC II and ALVIN-based studies of faulting on the East Pacific Rise 9°20'N-9°50'N: Marine Geophysical Researches, v. 18, no. 5, p. 557-587.

Ballard, R. D., and Van Andel, T. H., 1977, Morphology and tectonics of the inner rift valley at lat 36°50'N on the Mid-Atlantic Ridge: Geological Society of America Bulletin, v. 88, p. 507-530.

Behn, M. D., Lin, J., and Zuber, M. T., 2002, Mechanisms of normal fault development at mid-ocean ridges: Journal of Geophysical Research, v. 107, no. B4, p. 7.1-7.18.

Bonatti, E., and Harrison, C. G. A., 1988, Eruption styles of basalt in oceanic spreading ridges and seamounts: Effect of magma temperature and viscosity: Journal of Geophysical Research, v. 93, p. 2,967-2,980.

Cann, J. R., and Smith, D. K., 2005, Evolution of volcanism and faulting in a segment of the Mid-Atlantic Ridge at 25°N: Geochemistry, Geophysics, Geosystems, v. 6, no. 9, p. 1-20.

Cave, R. R., German, C. R., Thomson, J., and Nesbitt, R. W., 2001, Fluxes to sediments underlying the Rainbow hydrothermal plume at 36º14'N on the Mid-Atlantic Ridge: Geochemica et Cosmochimica Acta, v. 66, no. 11, p. 1905-1923.

Dziak, R. P., Smith, D. K., Bohnenstiehl, D. R., Fox, C. G., Desbruyeres, D., Matsumoto, H., Tolstoy, M., and Fornari, D. J., 2004, Evidence of a recent magma dike intrusion at the slow spreading Lucky Strike segment, Mid-Atlantic Ridge: Journal of Geophysical Research, v. 109, no. B12102, p. 1-15.

Escartin, J., Cannat, M., Pouliquen, G., and Rabain, A., 2001, Crustal thickness of V-shaped ridges south of the Azores: Interaction of the Mid-Atlantic Ridge (36°-39°) and the Azores hot spot: Journal of Geophysical Research, v. 106, no. B10, p. 21,719-21,735.

Escartin, J., Cowie, P., Searle, R., Allerton, S., Mitchell, N., MacLEod, C., and Slootweg, A., 1999, Quantifying tectonic strain and magmatic accretion at a slow spreading ridge segment, Mid-Atlantic Ridge, 29°N: Journal of Geophysical Research, v. 104, no. B5, p. 10,421-10,437.

Escartin, J., Soule, S. A., Bezos, A., Cannat, M., Fornari, D. J., Ballu, V., and Humphris, S. E., 2006, Patterns of volcanism and tectonism at a slow-spreading segment of the Mid-Atlantic Ridge (Lucky Strike, 37°N): preliminary results from near-bottom geological and geophysical surveys: Eos, Transactions, American Geophysical Union, v. 87, no. 52, Fall Meet., Suppl., Abstract.

Escartin, J., Soule, S. A., Fornari, D. J., Tivey, M. A., Schouten, H., and Perfit, M. R., 2007, Interplay between faults and lava flows in construction of the upper oceanic crust: The East Pacific Rise crest 9°25'N-9°58'N: Geochemistry, Geophysics, Geosystems, v. 8, no. 6, p. 20.

Fornari, D. J., and Humphris, S. E., 1996, LUSTRE'96, Final Cruise Report, p. 41pp w/Appendices.

Gracia, E., and Escartin, J., 1999, Crustal accretion at mid-ocean ridges and backarc spreading centers: insights from the Mid-Atlantic Ridge, the Bransfield Basin and the North Fiji Basin: Contributions to Science, v. 1, no. 2, p. 175-187.

Gregg, T. K. P., and Fink, J. H., 1995, Quantification of submarine lava-flow morphology through analog experiments: Geology, v. 23, p. 73-76.

Gross, M. R., and Engelder, T., 1995, Strain accomodated by brittle fault failure in adjacent units of the Monterey Formation, U.S.A.: scale effects and evidence for uniform displacement boundary conditions: Journal of Structural Geology, v. 17, no. 9, p. 1303-1318.

Humphris, S., Fornari, D. J., Scheirer, D. S., German, C. R., and Parson, L. M., 2002, Geotectonic Setting of hydrothermal activity on the summit of Lucky Strike Seamount (37°17'N, Mid Atlantic Ridge: Geochemistry, Geophysics, Geosystems, v. 3, no. 8, p. 1-24.

Kennish, M. J., and Lutz, R. A., 1998, Morphology and distribution of lava flows on mid-ocean ridges: a review: Elsevier Science, v. 43, p. 63-90.

Kent, G. M., Harding, A. J., and Orcutt, J. A., 1993, Distribution of magma beneath the East Pacific Rise between Clipperton Transform and the 9°17'N deval from forward modeling of common depth point data: Journal of Geophysical Research, v. 98, p. 13,945-13,969.

Langmuir, C., Humphris, S. E., Fornari, D. J., Van Dover, C., Von Damm, K., Tivey, M. K., Colodner, D., Charlou, J. L., Desonie, D., Wilson, C., Fouquet, Y., Klinkhammer, G., and Bougault, H., 1997, Hydrothermal vents near a mantle hot spot: the Lucky Strike vent field at 37°N on the Mid-Atlantic Ridge: Earth and Planetary Science Letters, v. 148, p. 69-91.

Lisitzin, A. P., 1972, Sedimentation in the World Ocean, With Emphasis on the Nature, Distribution, and Behavior of Marine Suspensions, Society of Economic Paleontologists and Mineralogists, 218 p.

MacDonald, K. C., and Luyendyk, B. P., 1977, Deep-tow studies of the structure of the Mid-Atlantic Ridge crest near lat 37°N: Geological Society of America Bulletin, v. 88, p. 621-636.

Magde, L. S., and Smith, D. K., 1995, Seamount volcanism at the Reykjanes Ridge: Relationship to the Iceland hot spot: Journal of Geophysical Research, v. 100, no. B5, p. 8449-8468.

Marrett, R., and Allmendinger, R. W., 1992, Amount of extension on "small" faults: An example from the Viking graben: Geology, v. 20, p. 47-50.

McClain, J. S., Orcutt, J. A., and Burnett, M., 1985, The East Pacific Rise in cross section: a seismic model: Journal of Geophysical Research, v. 90, no. B10, p. 8,627-8,640.

Mitchell, N. C., 1993, A Model for Attenuation of Backscatter due to Sediment Accumulations and Its Application to Determine Sediment Thickness with GLORIA Sidescan Sonar: Journal of Geophysical Research, v. 98, no. B12, p. 22,477-22,493.

Navin, D. A., Pierce, C., and Sinha, M. C., 1998, The RAMESSES experiment--II. Evidence for accumulated melt beneath a slow spreading ridge from wide-angle refraction and multichannel reflection seismic profiles: Geophysical Journal International, v. 135, p. 746-772.

Nozaki, Y., Cochran, J. K., Turekian, K. K., and Keller, G. H., 1977, Radiocarbon and ^{210}Pb distribution in submersible-taken deep-sea cores from Project FAMOUS: Earth and Planetary Science Letters, v. 34, p. 167-173.

Ondreas, H., Fouquet, Y., Voisset, M., and Radford-Knoery, J., 1997, Detailed Study of Three Contiguous Segments of the Mid-Atlantic Ridge, South of the Azores (37° N to 38°30' N), Using Acoustic Imaging Coupled with Submersible Observations: Marine Geophysical Researches, v. 19, p. 231-255.

Parson, L. M., Gracia, E., Coller, D., German, C. R., and Needham, D., 2000, Second-order segmentation; the relationship between volcanism and tectonism at the MAR, 38°-35°40'N: Earth and Planetary Science Letters, v. 178, p. 231-251.

Perfit, M. R., and Chadwick, W. W., 1998, Magmatism at Mid-Ocean Ridges: Constraints from Volcanological and Geochemical Investigations, *in* Buck, W. R., Delaney, P. T., Karson, J. A., and Lagabrielle, Y., eds., Faulting and Magmatism at Mid-Ocean Ridges: Washington, D.C., American Geophysical Union, p. 59-115.

Pierce, C., Gardiner, A., and Sinha, M. C., 2005, Temporal and spatial cyclicity of accretion at slow-spreading ridges--evidence from the Reykjanes Ridge: Geophysical Journal International, v. 163, p. 56-78.

Pierce, C., and Navin, D. A., 2002, The RAMESSES experiment--V Crustal Accretion at axial volcanic ridge segments--a gravity study at 57º 45'N on the slow spreading Reykjanes Ridge: Geophysical Journal International, v. 149, p. 76-49.

Ramberg, I. B., Gray, D. F., and Raynolds, R. G. H., 1977, Tectonic Evolution of the FAMOUS area of the Mid-Atlantic Ridge, lat 35°50'N-37°20'N: Geological Society of America Bulletin, v. 88, p. 609-620.

Ruddiman, W. F., 1972, Sediment Redistribution on the Reykjanes Ridge: Seismic Evidence: Geological Society of America Bulletin, v. 83, p. 2039-2062.

Scheirer, D. S., Fornari, D. J., Humphris, S. E., and Lerner, S., 2000, High-resolution seafloor mapping using the DSL-120 sonar system: Quantitative assessment of sidescan and phase-bathymetry data from the Lucky Strike segment of the Mid-Atlantic Ridge: Marine Geophysical Researches, v. 21, p. 121-142.

Searle, R. C., Cowie, P. A., Mitchell, N. C., Allerton, S., MacLeod, C., Escartin, J., Russell, S. M., Slootweg, P. A., and Tanaka, T., 1998, Fault structure and detailed evolution of a slow-spreading ridge segment: the Mid-Atlantic Ridge at 29°N: Earth and Planetary Science Letters, v. 154, p. 167-183.

Singh, S. C., Crawford, W. C., Carton, H., Seher, T., Combier, V., Cannat, M., Canales, J. P., Dusunur, D., Escartin, J., and Miranda, J. M., 2006, Discovery of a magma chamber and faults beneath a Mid-Atlantic Ridge hydrothermal field: Nature, v. 442, no. 31, p. 1029-1032.

Sinha, M. C., Constable, S. C., Pierce, C., White, A., Heinson, G., MacGregor, L. M., and Navin, D. A., 1998, Magmatic processes at slow spreading ridges; implications of the RAMESSES experiment at 57º 45'N on the Mid-Atlantic Ridge: Geophysical Journal International, v. 135, p. 731-745.

Smith, D. K., and Cann, J. R., 1990, Hundreds of small volcanoes on the median valley floor of the Mid-Atlantic Ridge at 24-30°N: Nature, v. 348, p. 152-155.

Smith, D. K., Cann, J. R., Dougherty, M. E., Lin, J., Spencer, S., MacLeod, C., Keeton, J., McAllister, E., Brooks, B., Pascoe, R., and Robertson, W., 1995, Mid-Atlantic Ridge volcanism from deep-towed side-scan sonar images, 25°-29°N: Journal of Volcanology and Geothermal Research, v. 67, p. 233-262.